RIS-Enabled Multi-user M-QAM Uplink NOMA Systems: Design, Analysis, and Optimization

Mahmoud AlaaEldin, *Member*, *IEEE*, Mohammad Al-Jarrah, *Member*, *IEEE*, Xidong Mu, *Member*, *IEEE*, Emad Alsusa, *Senior Member*, *IEEE*, Karim G. Seddik, *Senior Member*, *IEEE*, and Michail Matthaiou, *Fellow*, *IEEE*

***Abstract*—Non-orthogonal multiple access (NOMA) is widely recognized for enhancing the energy and spectral efficiency through effective radio resource sharing. However, uplink NOMA systems face greater challenges than their downlink counterparts, as their bit error rate (BER) performance is hindered by an inherent error floor due to error propagation caused by imperfect successive interference cancellation (SIC). This paper investigates the BER performance improvements enabled by reconfigurable intelligent surfaces (RISs) in multi-user uplink NOMA transmission. Specifically, we propose a novel RIS-assisted uplink NOMA design, where the RIS phase shifts are optimized to enhance the received signal amplitudes while mitigating the phase rotations induced by the channel. To achieve this, we first develop an accurate channel model for the effective user channels, which facilitates our BER analysis. We then introduce a channel alignment scheme for a two-user scenario, enabling efficient SIC-based detection and deriving closed-form BER expressions. We further extend the analysis to a generalized setup with an arbitrary number of users and modulation orders for quadrature amplitude modulation signaling. The analysis is also extended to consider imperfect channel state information (CSI) knowledge and the multi-antenna base station (BS) cases. Using the derived BER expressions, we develop an optimized uplink NOMA power allocation (PA) scheme to minimize the average BER while satisfying the user transmit power constraints. It will be shown that the proposed NOMA detection scheme, in conjunction with the optimized PA strategy, eliminate SIC error floors at the base station. The theoretical BER expressions are validated using simulations, which confirms the effectiveness of the proposed design in eliminating BER floors.**

***Index Terms*—Bit error rate, power allocation, reconfigurable intelligent surfaces, uplink NOMA.**

I. Introduction

In recent years, there has been a pressing demand for high-data-rate communications which requires efficient utilization of the wireless resources. To address this challenge, non-orthogonal multiple access (NOMA) has been proposed as a revolutionary multiple-access technique that can in theory enhance the spectral efficiency. As a result, NOMA has gained significant attention from both academia and industry and is regarded a key candidate for future sixth-generation (6G) networks and beyond [1]–[3]. NOMA is categorized into two main schemes: power-domain NOMA and code-domain NOMA. In the former, users are assigned different power levels based on their channel conditions to the base station (BS), while in the latter, each user is assigned a unique code as a signature. This paper focuses on power-domain NOMA, where multiple devices share the same time-frequency resource block with different power levels, and successive interference cancellation (SIC) is employed at the receiver to effectively decode the signals [4].

Likewise, reconfigurable intelligent surfaces (RISs) have emerged in recent years as smart technology capable of improving the quality of wireless communication links [5]–[9]. An RIS typically consists of a large number of low-cost, tunable passive elements that can adjust the amplitudes and phase shifts of incident waves, effectively reflecting or refracting them toward the receiver. The key advantage of RISs lies in their ability to customize the wireless channel to support various critical features, such as signal enhancement and interference mitigation. Consequently, the integration of RISs into diverse wireless systems has been extensively studied in recent literature. For example, in [10], the authors developed alternation minimization algorithms to minimize the total transmit power by jointly optimizing the active beamforming at the BS and the passive beamforming at the RIS. In [11], the maximization of the energy efficiency (EE) of RIS-assisted downlink systems was considered. Furthermore, in [12], a joint power and user association scheme was proposed for a multi-RIS-assisted multi-BS system using mm-Wave. Other applications of RISs span various topics in wireless communications, such as physical layer network coding [13], unmanned ariel vehicles (UAV) communications [14], collaborative jamming and anti-jamming networks [15], and throughput and energy efficiency optimization for uplink NOMA networks [16].

A. Related work

Since NOMA is capable of approaching the boundary of the capacity region, multiple works in the literature have studied the integration of NOMA in RIS-enabled systems as a win-win solution [17], [18]. In the following, we provide a review of the literature focusing on the performance analysis of uplink RIS-NOMA systems.

The authors of [19] studied the outage performance of a simplified RIS enabled uplink two-user NOMA system.

This work was supported by the U.K. Engineering and Physical Sciences Research Council (EPSRC) grant (EP/X04047X/2) for TITAN Telecoms Hub and the European Research Council (ERC) under the European Union's Horizon 2020 Research and Innovation Programme (grant agreement No. 101001331).

Mahmoud AlaaEldin, Xidong Mu, and Michail Matthaiou are with the Centre for Wireless Innovation (CWI), Queen's University Belfast, Belfast BT3 9DT, U.K. (e-mail: m.alaaeldin@qub.ac.uk; x.mu@qub.ac.uk; m.matthaiou@qub.ac.uk).

Mohammad Al-Jarrah and Emad Alsusa are with the Electrical and Electronic Engineering Department, University of Manchester, Manchester M13 9PL, U.K. (e-mail: mohammad.al-jarrah@manchester.ac.uk; e.alsusa@manchester.ac.uk).

Karim G. Seddik is with the Department of Electronics and Communications Engineering, American University in Cairo, Cairo, Egypt 11835 (e-mail: kseddik@aucegypt.edu).

Specifically, they derived approximate analytical expressions for the received powers of the NOMA users as Gamma random variables (RVs) using the method of moment matching, which resulted in tractable expressions of the outage probability with SIC. In addition, the study in [20] analyzed the outage performance of a RIS-assisted two-user uplink NOMA system, which divided the RIS elements into two groups to improve each user's signal. By approximating the received powers as Gamma RVs, they derived outage probability expressions for uplink NOMA signaling using SIC. The authors of [21] investigated downlink and uplink RIS-aided NOMA and orthogonal multiple access (OMA) systems, where an RIS is applied to enhance the coverage for a cell-edge user communicating with the BS. Closed-form expressions for the outage probability and ergodic rate under Nakagami-m fading have been derived. Using asymptotic approximations in the high signal-to-noise-ratio (SNR) regime, it has been revealed that there is a diversity order that depends on the number of RIS elements and fading parameters, while the high SNR slope is unaffected. In [22], the authors studied the symbol error rate (SER) performance of simultaneously transmitting and reflecting reconfigurable intelligent surface (STAR-RIS)-aided uplink NOMA, where the phase shift and amplitude parameters were adjusted based on distance-maximizing constellation scaling and rotation to enhance the SER performance of the system. However, closed-form SER expressions were not derived in [22] as the expressions are given by K-fold integrals. Finally, the authors of [23] investigated the ergodic sum-rate of the STAR-RIS-assisted uplink NOMA under channel estimation errors and hardware impairments, where upper bounds were derived for perfect and imperfect SIC-based decoding.

On the other hand, the analysis of RIS-enabled downlink NOMA systems has also been investigated in the literature. However, most of the existing work focused on the analysis of ergodic capacity and outage probability, such as [24]–[28], although the error rate analysis is the most revealing metric of the system performance. Few other works have studied the error rate analysis of downlink RIS-NOMA systems to fill this gap [26], [29]–[31]. Nevertheless, the existing works have focused on downlink scenarios under restrictive assumptions, such as fixed numbers of users or low-order modulation schemes. For instance, some studies addressed only specific cases like four-user binary phase shift keying (BPSK) systems [26], approximated error performance through union bounds without accurately capturing SIC error propagation [30], or limited their analysis to two-user constellations with only quadrature phase shift keying (QPSK) and BPSK [29].

Downlink RIS-NOMA approaches overlook the general uplink case, where SIC errors depend critically on individual users' channels and directly contribute to bit error rate (BER) floors. In downlink RIS-NOMA, user signals are superimposed at the BS and pass through the same channel to all users, forming a structured constellation without error floors. However, in uplink RIS-NOMA, signals traverse different user channels before reaching the BS, causing stronger inter-user interference at high SNR and leading to BER floors. This gap motivates the need for a comprehensive BER analysis and optimization framework for uplink RIS-NOMA that accommodates arbitrary modulation orders and user numbers.

	Our work	[19]	[20]	[21]	[22]	[23]
RIS-NOMA	✓	✓	✓	✓	✓	✓
Uplink	✓	✓	✓	✓	✓	✓
BER analysis	✓	✗	✗	✗	✗	✗
Arbitrary # of users	✓	✗	✗	✗	✗	✗
Arbitrary Mod. orders	✓	✗	✗	✗	✗	✗
BER-based uplink PA	✓	✗	✗	✗	✗	✗

Table I: Distinguishing the work in this paper from other existing works in the literature

B. Motivations and Contributions

From the literature review, it is evident that most of the existing works have focused on the analysis of the achievable rate and outage capacity of RIS-enabled uplink NOMA systems. To the best of the authors' knowledge, the investigation of reliability metrics, such as BER, has not been considered in the literature. Studying the BER performance analysis is indispensable for characterizing the reliability of communication systems, as it helps to predict the error rate of the received data, which has a direct impact on the effective throughput of communication links. Therefore, to bridge this clear gap in the literature, this paper provides a comprehensive study of the BER performance limits of uplink RIS-NOMA systems under imperfect SIC. Similar to existing literature [19], [20], [23], [30], the RIS is partitioned into K partitions, where K is the number of users, and each partition is assigned to a certain user. Then, the phase shifts of each RIS partition are adjusted to maximize the effective channel of the corresponding user. This partitioning technique allows us to statistically model the effective channels of the users which is required to derive the average BER analytical expressions.

The key contributions of this work are summarized as follows:

- A detailed and accurate statistical modeling of the effective channels of the users is introduced under Ricean fading based on dividing the RIS panel into K partitions and assigning each partition to a certain user. The deterministic line-of-sight (LoS) components of the Ricean channels are even accurately described to capture the elevation and azimuth angles of each user to the RIS and the LoS of the RIS-BS link.
- A novel channel alignment scheme is then devised to align the effective channels of the users on the real axis to eliminate the relative phase shifts between the effective channels of the users. This allows for the construction of a simple and tractable SIC-based detection of the users' symbols at the BS. The proposed channel alignment facilitates the BER performance analysis of the two-user uplink RIS-NOMA scenario.
- An extension of the BER analysis is conducted for the case of arbitrary number of users and quadrature amplitude modulation (QAM) modulation orders, providing valuable insights on the achievable performance of the RIS-NOMA system. This is done by devising an algorithm that computes the coefficients of the BER expressions for any system with arbitrary parameters.

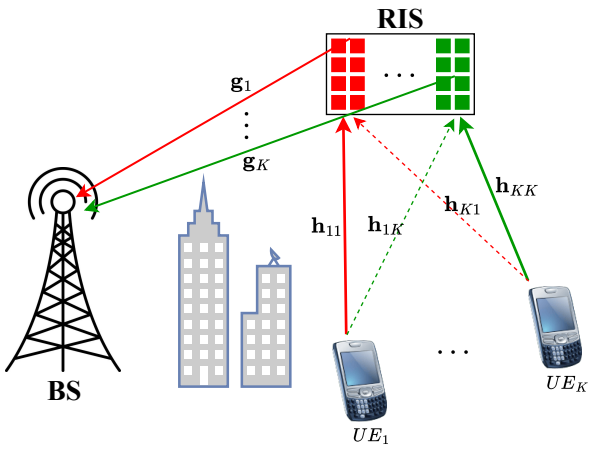

Figure 1: RIS-enabled uplink NOMA system model

- The BER analysis is further extended to consider the imperfect channel state information (CSI) knowledge and the multi-antenna BS cases.
- A power allocation (PA) scheme that utilizes the derived BER expressions is devised to eliminate the BER floors, by minimizing the average BER of all users subject to individual uplink transmit power constraints for the users.
- Simulation results verify the accuracy and effectiveness of the proposed closed-form generic analytical BER expressions. The results also reveal the efficacy of the proposed PA scheme, showing that it completely eliminates the BER floors. Moreover, we compare RIS-NOMA systems with the equivalent RIS-OMA counterparts. The results confirm the superiority of RIS-NOMA over RIS-OMA across all scenarios and all SNR values when both systems maintain the same channel estimation overhead for a fair comparison.

Finally, Table I explicitly contrasts our contributions to the existing works on RIS-NOMA in the literature.

C. Organization and Notations

The rest of the paper is organized as follows: In Sec. II, the RIS-enabled uplink NOMA system model is presented. The statistical modeling and channel alignment of the RIS uplink channels is presented in Sec. III. In Sec. IV, we present the BER analysis of the two-user uplink RIS-NOMA system, whereas the analysis is extended in Sec. V for the generalized system with an arbitrary number of NOMA users and arbitrary modulation orders. An optimized uplink PA scheme for the uplink RIS-NOMA system is discussed in Sec. VIII. The simulation results and discussion are given in Sec. IX, while the conclusions of this work are presented in Sec. X.

Notations: The bold lowercase letters are used to define vectors, while the bold uppercase letters are used to define matrices. The symbols $|\cdot|$, $\mathfrak{Re}(\cdot)$, $\mathfrak{Im}(\cdot)$, $\arg(\cdot)$, and $(\cdot)^*$ denote the absolute, real, imaginary, angle, and conjugate of a complex number, while $j'=\sqrt{-1}$ is the imaginary number.

II. System Model

As shown in Fig. 1, we consider an uplink RIS-enabled NOMA system that contains a single antenna BS, an RIS with L reflectors, and K single antenna users, where the ith user is denoted by U_i. In our proposed design, we assume that the RIS is divided into separate K partitions, denoted as $\mathcal{P}_1, \mathcal{P}_2, \cdots, \mathcal{P}_K$, where partition $\mathcal{P}_i$ is assigned to U_i and contains L_i reflection elements of the RIS, i.e., $\sum_{k=1}^{K} L_i = L$. The RIS phase shifts of each partition are adjusted to align the channels of the corresponding user so that the received signal components of each user are coherently added at the destination. As shown in Fig. 1, the channel vector from U_i to its associated RIS partition, $\mathcal{P}_i$, is denoted as $\mathbf{h}_{ii} \in \mathbb{C}^{L_i \times 1}$. On the other hand, the cross channel vector from U_i to the partition $\mathcal{P}_j$ is denoted as $\mathbf{h}_{ij} \in \mathbb{C}^{L_j \times 1}$. Moreover, the channel vector from the ith portion, $\mathcal{P}_i$, to the BS is denoted as $\mathbf{g}_i \in \mathbb{C}^{L_i \times 1}$, while the direct link from U_i to the BS is v_i. Therefore, the received superimposed NOMA signal, y, at the BS can be expressed as

$$y = \sum_{i=1}^{K} \sqrt{P_i/\beta_i} \left(\sum_{j=1}^{K} \sqrt{\eta_i} \mathbf{h}_{ij}^T \mathbf{\Theta}_j \mathbf{g}_j + \sqrt{\eta_i^{\text{dir}}} v_i \right) x_i + n, \tag{1}$$

where P_i denotes the transmit power of U_i, η_i represents the overall path loss of the cascaded channel, i.e., user-RIS-BS link, and $\mathbf{\Theta}_j$ is a diagonal matrix whose diagonal elements are the $\mathcal{P}_j$ reflection coefficients, i.e., $\mathbf{\Theta}_j = \text{diag}\{e^{j'\theta_{j,1}}, e^{j'\theta_{j,2}}, \ldots, e^{j'\theta_{j,L_j}}\}$, with $\theta_{j,l}$ representing the phase shift introduced by the lth reflecting element of $\mathcal{P}_j$. The term $x_i \in \mathbb{C}$ denotes the transmitted modulation symbol of U_i, drawn from a QAM alphabet, $\mathcal{X}_i$, where the cardinality of $\mathcal{X}_i$ is the QAM modulation order of U_i. The real and imaginary components of x_i can take values from the set $\{\pm 1, \pm 3, \ldots, \pm\sqrt{M_i} - 1\}$ in the square QAM case, while in the rectangular QAM case, the real component can take the values $\{\pm 1, \pm 3, \ldots, \pm\sqrt{2M_i} - 1\}$ while the imaginary component has the values $\{\pm 1, \pm 3, \ldots, \pm\sqrt{M_i/2} - 1\}$, where M_i is the modulation order of U_i. The scaling factor, β_i, is used to normalize x_i to unity, where it can be expressed as $\beta_i = \frac{2}{3}(M_i - 1)$ in the case of the square QAM. The parameter, $\eta_i = \eta_{U_i,I}\eta_{I,B}$, in (1) is the overall path loss of the U_i-RIS-BS link, where $\eta_{U_i,I} = d_{U_i,I}^{-\psi}$, $\eta_{I,B} = d_{I,B}^{-\psi}$; $d_{U_i,I}$ is the distance between the ith user and RIS, $d_{I,B}$ is the BS-RIS distance, where ψ is the path loss exponent of the wireless links of the RIS. $\eta_i^{\text{dir}} = d_{U_i,BS}^{-\psi^{\text{dir}}}$ is the path loss of the direct link of U_i, where $d_{U_i,BS}$ is the distance between U_i and the BS, and ψ^{dir} is the path loss exponent of the direct links. The additive white Gaussian noise at BS is denoted by n, and it is modeled as a complex Gaussian RV with zero mean and variance of σ_n^2 *per complex dimension*, i.e., $n \sim \mathcal{CN}(0, 2\sigma_n^2)$. The direct links are modeled as Rayleigh fading channels, thus v_i is a complex Gaussian RV, i.e., $v_i \sim \mathcal{CN}(0, 1)$. The channel vectors $\mathbf{g}_j$ and $\mathbf{h}_{ij}, \forall i, j$ are assumed to be Ricean fading channels, and they can be expressed as

$$\mathbf{h}_{ij} = \sqrt{K_1/K_1+1}\,\mathbf{h}_{ij}^{LoS} + \sqrt{1/K_1+1}\,\mathbf{h}_{ij}^{NLoS}, \tag{2}$$

$$\mathbf{g}_j = \sqrt{K_2/K_2+1}\,\mathbf{g}_j^{LoS} + \sqrt{1/K_2+1}\,\mathbf{g}_j^{NLoS}, \tag{3}$$

where K_1 and K_2 denote the Ricean factors, $\mathbf{h}_{ij}^{LoS}$ and $\mathbf{g}_j^{LoS}$ are the LoS components, and $\mathbf{h}_{ij}^{NLoS}$ and $\mathbf{g}_j^{NLoS}$ are the non-LoS (NLoS) components of $\mathbf{h}_{ij}$ and $\mathbf{g}_j$, respectively. The elements of $\mathbf{h}_{ij}^{NLoS}$ and $\mathbf{g}_j^{NLoS}$ are independent and

identically distributed (i.i.d.) complex normal, $\mathcal{CN}(0,1)$, RVs. Let us assume that the RIS is located in the $x-z$ plane and is composed of $L = L_x \times L_z$ antenna elements, where $L_x = 2\tilde{L}_x+1$ and $L_z = 2\tilde{L}_z+1$. The antenna spacings along the two directions are denoted by d_x and d_z, respectively. Thus, the deterministic LoS components of the channel vectors can be expressed as

$$\mathbf{a}^{LoS}(\Psi,\Omega) = \left[e^{-j\frac{2\pi}{\lambda}\tilde{N}_x d_x \cos\Psi \sin\Omega}, \ldots, e^{j\frac{2\pi}{\lambda}\tilde{N}_x d_x \cos\Psi \sin\Omega}\right]^T \otimes \left[e^{-j\frac{2\pi}{\lambda}\tilde{N}_z d_z \cos\Omega}, \ldots, e^{j\frac{2\pi}{\lambda}\tilde{N}_z d_z \cos\Omega}\right]^T, \quad (4)$$

where $\mathbf{a}\in\{\mathbf{h}_{ij}, \mathbf{g}_j\}$, and Ψ and Ω denote the azimuth and elevation angles of the receiver with respect to the $x-z$ plane, respectively.

The BS is assumed to have CSI knowledge of the cascaded channel vector $\mathbf{h}_{ii} \circ \mathbf{g}_i, \forall i$ [32]–[34], so that the phase shifts of the RIS reflection elements can be configured to reflect incident signals with concentrated beams towards the BS. It should be noted that there is no need for the estimation of the channels of all RIS elements to the users, i.e., knowledge of the cross channel vectors, $\mathbf{h}_{i,j}, \forall i \neq j$, is not required. Since the ith user, U_i, is assigned a separate partition of the RIS, $\mathcal{P}_i$, the phase shifts of $\mathcal{P}_i$ are adjusted to maximize the reflected signal from $\mathcal{P}_i$ at the BS. However, U_i signal reflections from other RIS partitions, $\mathcal{P}_j, \forall j \neq i$, are considered random signal reflections, since the phase shifts of these partitions are not adjusted to the U_i channels. Therefore, two signal components of U_i are received at the BS, namely, the optimized component and the random component. To maximize the reflected signal component of $\mathcal{P}_i$ received at the BS, the adjustable phase shifts of $\mathcal{P}_i$ are set as $\theta_{i,l} = -(\arg(h_{ii,l})+\arg(g_{i,l})), \forall l = 1, \ldots, L_i$, where $\theta_{i,l}$ is the phase shift of the lth reflection element of $\mathcal{P}_i$, and $h_{ii,l}$ and $g_{i,l}$ are the lth elements of $\mathbf{h}_{ii}$ and $\mathbf{g}_i$, respectively. As a result, the total received superimposed signal at the BS can be written as

$$y = \sum\nolimits_{i=1}^{K} \left(\gamma_{ii} + \sum\nolimits_{j=1, j\neq i}^{K} \gamma_{ij} + \sqrt{\eta_i^{\text{dir}}} v_i\right) x_i + n, \quad (5)$$

where γ_{ii} is the optimized component of the RIS effective channel of the ith user, reflected from its allocated partition, $\mathcal{P}_i$, which can be expressed as

$$\gamma_{ii} = \sqrt{P_i \eta_i / \beta_i} \sum\nolimits_{l=1}^{L_i} |h_{ii,l}||g_{i,l}|. \quad (6)$$

The terms, $\gamma_{ij}=\sqrt{P_i\eta_i/\beta_i}\widetilde{\gamma}_{ij}, \forall j\neq i$, are the random components of the RIS effective channel of user i, reflected from the other users' partitions, $\mathcal{P}_j, \forall j\neq i$, where $\widetilde{\gamma}_{ij}$ is the normalized random component and can be expressed as

$$\widetilde{\gamma}_{ij} = \sum\nolimits_{l=1}^{L_j} h_{ij,l}|g_{j,l}|e^{-j'\arg(h_{jj,l})}, \quad \forall i, j, \ i \neq j, \quad (7)$$

where $h_{ij,l}$ is the lth element of $\mathbf{h}_{ij}$, and $g_{j,l}$ is the lth element of $\mathbf{g}_j$. It should be noted that we order the users based on their distances to the RIS for SIC ordering. The effective channel power levels of the users mainly depend on the optimized components γ_{ii}, and due to RIS channel hardening, SIC ordering based on the distances will be violated with only low probability. Moreover, the proposed PA in Sec. VIII ensures sufficiently distant received signal powers, keeping the probability of instantaneous SIC ordering violations very low.

In the next section, we provide an accurate statistical modeling for the RIS effective channels and a channel alignment scheme to align the effective channels of the users. This will be used to derive closed-form average BER expressions in the subsequent sections.

III. Statistical modeling and alignment of the RIS effective channels of the users

In this section, accurate statistical modeling is derived for both the optimized component, γ_{ii}, and the random components, γ_{ij}, of the RIS effective channel of the ith user. Moreover, a channel alignment scheme is devised to align the effective channels of the users to the zero axis, which later facilitates simple detection and the BER derivations. The statistical models of the channel components derived in this section will be used in Sec. IV and Sec. V for the calculation of the unconditional average BER of the users at BS.

A. Statistical modeling of the effective channels of the users

The optimized component, γ_{ii}, is a summation of cascaded i.i.d. Rayleigh RVs, as in (6), which can be modeled as a Gamma RV using moment matching according to the casual form of the central limit theorem (CLT) [20], [35].[1] Since both $h_{ii,l}$ and $g_{i,l}$ in (6) are independent non-central complex Gaussian RVs, their envelopes are distributed as Ricean RVs. The mean value of a Ricean RV is given as [36]

$$\mu_{Rice} = \sigma\sqrt{\pi/2}\mathcal{L}_{1/2}(-\nu^2/2\sigma^2), \quad (8)$$

where $\nu=\sqrt{K/(K+1)}$ is the amplitude of the LoS component of the Ricean channel, $\sigma^2=1/(2(K+1))$ is the variance per dimension of the NLoS component, and $\mathcal{L}_q(\cdot)$ denotes a Laguerre polynomial. Hence, the mean value of γ_{ii} can be derived using the mean formula of the Ricean RV [36] as

$$\mathbb{E}(\gamma_{ii}) = \sqrt{\frac{P_i\eta_i}{\beta_i}} L_i \mathbb{E}(|h_{ii,l}||g_{i,l}|) = \sqrt{\frac{P_i\eta_i}{\beta_i(K_1+1)(K_2+1)}} \times \frac{\pi}{4} L_i \mathcal{L}_{1/2}(-K_1)\mathcal{L}_{1/2}(-K_2). \quad (9)$$

Moreover, the variance of the product of two Ricean RVs, $|h_{ii,l}||g_{i,l}|$, can be calculated as

$$\text{Var}(|h_{ii,l}||g_{i,l}|) = \mathbb{E}\left(|h_{ii,l}|^2\right)\mathbb{E}\left(|g_{i,l}|^2\right) - \mathbb{E}(|h_{ii,l}|)^2\mathbb{E}(|g_{i,l}|)^2 = 1 - \frac{1}{(K_1+1)(K_2+1)}\frac{\pi^2}{16}\mathcal{L}_{1/2}^2(-K_1)\mathcal{L}_{1/2}^2(-K_2), \quad (10)$$

where $\mathbb{E}\left(|h_{ii,l}|^2\right) = \mathbb{E}\left(|g_{i,l}|^2\right) = \nu^2 + 2\sigma^2 = 1$. Thus, the variance of γ_{ii} can be given as $\text{Var}(\gamma_{ii}) = \frac{P_i\eta_i}{\beta_i} L_i \text{Var}(|h_{ii,l}||g_{i,l}|)$.

Let us define the scale and shape parameters of the equivalent Gamma RV by ζ and N, respectively. Then, γ_{ii} has a

[1] It should be noted that the sum of the RIS cascaded channels, modeled as the sum of i.i.d. double Ricean/Rayleigh processes, is tightly approximated by a Gamma random variable obtained via moment matching. This is indeed a well-established approach reported in the literature [19], [20], [24], [30], [35].

mean value of $N\zeta$ and a variance of $N\zeta^2$ [36]. Therefore, by equating the mean and variance of γ_{ii} to the mean and variance of the Gamma RV, both the scale and shape parameters of the Gamma RV can be derived as

$$\zeta_i = {}^{\mathrm{Var}(\gamma_{ii})}/_{\mathbb{E}(\gamma_{ii})}, \quad N_i = {}^{\mathbb{E}(\gamma_{ii})^2}/_{\mathrm{Var}(\gamma_{ii})}. \tag{11}$$

Finally, the characteristic function (CF) of γ_{ii} can be given as

$$\Phi_{\gamma_{ii}}(z) = (1 - j'\zeta_i z)^{-N_i}. \tag{12}$$

Now, we derive the statistics of the random components of the effective channels, γ_{ij}. To calculate the first and second moments of $\mathfrak{Re}(\widetilde{\gamma}_{ij})$ and $\mathfrak{Im}(\widetilde{\gamma}_{ij})$, we substitute $h_{ij,l}$ in (7) by using its LoS and NLoS components as

$$\widetilde{\gamma}_{ij} = \sum\nolimits_{l=1}^{L_j} |g_{j,l}| \Big(c_1 e^{j'\chi_l} + c_2 h_{ij,l}^{NLoS} e^{-j' \arg(h_{jj,l})} \Big), \tag{13}$$

where $c_1 = \sqrt{\frac{K_1}{K_1+1}}$, $c_2 = \sqrt{\frac{1}{K_1+1}}$, $\chi_l = -\arg(h_{jj,l}) + \phi_{ij,l}^{LoS}$ and $\phi_{ij,l}^{LoS}$ is the phase shift of the LoS path from user i to the lth element of $\mathcal{P}_j$. Given that $h_{ij,l}^{NLoS}$ is a zero mean complex normal RV, and χ_l can be modeled as a Von-Mises distribution, the expected value of the real part of the lth term of $\widetilde{\gamma}_{ij}$ can be expressed, using the trigonometric moments of the Von-Mises distribution derived in [37, Sec. 3.3 and Sec. 3.4], as

$$\begin{aligned} &\mathbb{E}(\mathfrak{Re}(\widetilde{\gamma}_{ij,l})) = c_1 \mathbb{E}(|g_{j,l}|)\mathbb{E}(\cos\chi_l) \\ &\approx c_1 \sqrt{\frac{\pi}{4(K_2+1)}} \mathcal{L}_{1/2}(-K_2) \frac{I_1(\kappa_1)}{I_0(\kappa_1)} \cos\left(\phi_{ij,l}^{LoS} - \phi_{jj,l}^{LoS}\right), \end{aligned} \tag{14}$$

where $I_n(\cdot)$ is the modified Bessel function of order n, and κ_1 is the concentration parameter of the Von-Mises RV, where it can be calculated by numerically solving ${}^{I_1(\kappa_1)}/_{I_0(\kappa_1)} = \sqrt{{}^{K_1}/_{K_1+1}}$ [37]. Similarly, $\mathbb{E}(\mathfrak{Im}(\widetilde{\gamma}_{ij}))$ has a similar expression as in (14) except that the cos function needs to be replaced by sin. Thus, $\mathbb{E}(\mathfrak{Re}(\widetilde{\gamma}_{ij})) = \sum_{l=1}^{L_j} \mathbb{E}(\mathfrak{Re}(\widetilde{\gamma}_{ij,l}))$.

Given that $\mathfrak{Re}\left(h_{ij,l}^{NLoS}\right)$ has zero mean and is independent of χ_l, the second moment of $\mathfrak{Re}(\widetilde{\gamma}_{ij,l})$ can be given, using the trigonometric moments of the Von-Mises distribution [37], as

$$\begin{aligned} &\mathbb{E}(\mathfrak{Re}(\widetilde{\gamma}_{ij,l})^2) = \mathbb{E}(|g_{j,l}|^2)\mathbb{E}\left(c_1^2\cos^2\chi + c_2^2 \mathfrak{Re}\left(h_{ij,l}^{NLoS}\right)^2\right) \\ &\approx \frac{c_1^2}{2}\left(1 + \frac{I_2(\kappa_1)}{I_0(\kappa_1)}\cos\left(2(\phi_{ij,l}^{LoS} - \phi_{jj,l}^{LoS})\right)\right) + \frac{c_2^2}{2}, \end{aligned} \tag{15}$$

where $\mathbb{E}(|g_{j,l}|^2)=1$. Therefore, the variance of $\mathfrak{Re}(\widetilde{\gamma}_{ij})$ can be given as

$$\mathrm{Var}(\mathfrak{Re}(\widetilde{\gamma}_{ij})) = \sum\nolimits_{l=1}^{L_j} \mathbb{E}\left(\mathfrak{Re}(\widetilde{\gamma}_{ij,l})^2\right) - \mathbb{E}(\mathfrak{Re}(\widetilde{\gamma}_{ij,l}))^2. \tag{16}$$

A weighted sum of i.i.d. RVs can converge to a Gaussian if the Lindeberg condition is satisfied, which states that the weights are not dominated by a few terms, i.e., no single weight is too large. This is our case in (13) since the weights, $\exp\left(j'(\phi_{ij,l}^{LoS} - \phi_{jj,l}^{LoS})\right)$, are unit-modulus complex numbers, which ensure that their real and imaginary parts are bounded numbers from -1 to 1. Thus, both $\mathfrak{Re}(\widetilde{\gamma}_{ij})$ and $\mathfrak{Im}(\widetilde{\gamma}_{ij})$ can be modeled as Gaussian RVs using CLT under the Lindeberg condition. Hence, the CF of $\mathfrak{Re}(\gamma_{ij})$ can be expressed as

$$\Phi_{\mathfrak{Re}(\gamma_{ij})}(z) = \exp\left(j'\mu_{\mathfrak{Re}(\gamma_{ij})}z - \sigma^2_{\mathfrak{Re}(\gamma_{ij})}z^2\right), \tag{17}$$

where $\mu_{\mathfrak{Re}(\gamma_{ij})} = \sqrt{{}^{P_i\eta_i}/_{\beta_i}}\mathbb{E}(\mathfrak{Re}(\widetilde{\gamma}_{ij}))$ and $\sigma^2_{\mathfrak{Re}(\gamma_{ij})} = {}^{P_i\eta_i}/_{\beta_i}\mathrm{Var}(\mathfrak{Re}(\widetilde{\gamma}_{ij}))$ are the mean and variance of $\mathfrak{Re}(\gamma_{ij})$, respectively.

B. Channel alignment scheme for the users' effective channels

In this subsection, we present an approach to align the overall effective channel of each user to the real axis by canceling the relatively small imaginary random components of the channel. This alignment scheme facilitates the efficient and simple detection of the uplink transmit data symbols of the users since it allows for simpler decision regions and decision thresholds. Moreover, obtaining closed-form expressions for BER becomes feasible using the proposed channel alignment scheme, since the received signal constellation of the superimposed NOMA symbols at the BS becomes a QAM-like constellation, allowing tractable BER analysis.

To align the effective channels of the users in (5), let us define the angles, $\alpha_j, \forall j \in \{1,\ldots,K\}$, as two control angles at the RIS. Specifically, α_j is set to control the RIS partition, $\mathcal{P}_j$, by rotating all its elements by the same value of α_j. Therefore, the received superimposed NOMA signal at the BS can be expressed as

$$y = \sum\nolimits_{i=1}^{K} \left(\sum\nolimits_{j=1}^{K} \gamma_{ij} e^{j'\alpha_j} + \sqrt{{}^{P_i\eta_i^{\mathrm{dir}}}/_{\beta_i} v_i} \right) x_i + n. \tag{18}$$

The angles $\alpha_j, \forall j$ are set so that they cancel the imaginary components of the overall effective channels of all the users, $h_i^{eff}, \forall i \in \{1,\ldots,K\}$. Hence, $\alpha_j, \forall j$ are calculated by simultaneously solving the following equations

$$\mathfrak{Im}\left(\sqrt{\eta_i} \sum\nolimits_{j=1}^{K} \widetilde{\gamma}_{ij} e^{j'\alpha_j} + \sqrt{\eta_i^{\mathrm{dir}}} v_i \right) = 0, \quad \forall i \in \{1,\ldots,K\}, \tag{19}$$

where the system of equations in (19) consists of K nonlinear equations in K unknown angles, $\alpha_j, \forall j$. To solve (19), the system of equations is transformed to a least-squares unconstrained minimization problem, as

$$\min_{\alpha_1,\ldots,\alpha_K} \quad \sum\nolimits_{i=1}^{K} \left(\mathfrak{Im}\left(\sum\nolimits_{j=1}^{K} \gamma_{ij} e^{j'\alpha_j} \right) \right)^2. \tag{20}$$

Problem (20) can be solved using one of the standard nonlinear optimization solvers, such as the trust-region algorithm [38], [39] or the well-known Levenberg–Marquardt algorithm [40] using a selected initial point. For problem (20), our simulations confirm that choosing all zeros for the angles, α_k, as an initial point always converges to a stationary minimal point of (20), where the value of the objective function is zero. Alternatively, the standard MATLAB numerical solver, fsolve, can be used to solve the nonlinear system of equations in (19).

Since the optimized components, $\gamma_{ii}, \forall i$, have much higher magnitude than the random components, $\gamma_{ij}, \forall i \neq j$, the solution for (19) would normally have small values for $\alpha_j, \forall j$. In other words, the overall effective channels of the users can be

aligned by adding a slight phase rotation to each RIS partition, which allows the large optimized channel components, $\gamma_{ii}, \forall i$, to dominate the small random components, $\gamma_{ij}, \forall i \neq j$. Thus, the overall effective channels of the users, $h_i^{eff}, \forall i$, become purely real after applying the control angles, α_j, and they can be written as

$$h_i^{eff} = \sum_{j=1}^{K} \gamma_{ij} e^{j' \alpha_j} \approx \gamma_{ii} + \sum_{\substack{j=1 \\ j \neq i}}^{K} \mathfrak{Re}(\gamma_{ij}), \quad \forall i \in \{1, \ldots, K\}, \tag{21}$$

where $\approx$ means approximately equal. Therefore, the CF of $h_i^{eff}, \forall i$, can be given using (12) and (17) as

$$\Phi_{h_i^{eff}}(z) \approx \Phi_{\gamma_{ii}}(z) \prod_{j=1, j \neq i}^{K} \Phi_{\mathfrak{Re}(\gamma_{ij})}(z). \tag{22}$$

The final received signal at the BS can then be expressed as

$$y = \sum_{i=1}^{K} h_i^{eff} x_i + n, \tag{23}$$

where $h_i^{eff}, \forall i$ are purely real RVs with zero phase rotations. In the next subsection, we show how the proposed channel alignment scheme facilitates the detection process and the BER analysis.

IV. BER ANALYSIS OF THE TWO-USER UPLINK RIS-NOMA SYSTEM

In this section, we provide a comprehensive BER analysis for the two-user RIS-NOMA scenario, assuming 16-QAM and QPSK modulation for U_1 and U_2, respectively. Gray coding is employed to map binary bits to modulation symbols for all modulation orders.

The symbols, x_1 and x_2, are jointly decoded from (23) based on the construction of the received superimposed NOMA symbol constellation at the BS. Given that the receiver noise, n, is circularly symmetric Gaussian, optimal detection simplifies to a minimum distance decoder based on the effective channel values, $h_i^{eff}, \forall i$. With zero phase rotations of the effective channels, the decision regions for the superimposed NOMA symbols are simple rectangular shapes, akin to standard QAM detection. This QAM-like constellation structure facilitates simple and tractable data decoding through simple thresholds and decision regions. Therefore, the decision thresholds can be calculated given h_1^{eff} and h_2^{eff}, as we show below. It should be noted that constructing simple and tractable decision regions facilitates the derivation of closed-form BER analytical expressions, which will be used later in optimizing the uplink PA to mitigate the ambiguity of the superimposed constellation of uplink NOMA and its associated BER floors.

The constellation of the 16-4-QAM NOMA symbols of the two-user system is shown in Fig. 2. The combined constellation diagram of the NOMA symbol in this case has 64 constellation points containing an information amount of 6 bits per symbol, that is, four bits for U_1 and two bits for U_2. Figure 2(a) divides the constellation points into two sets according to the value of b_{11} equal to 1 or 0, that is, the constellation points that have $b_{11} = 0$ are red colored, while the remaining points having $b_{11} = 1$ are in blue. Figure 2(b) divides the constellation diagram in the same way as Fig. 2(a) but according to b_{12}. For b_{13} and b_{14}, the constellation points are divided exactly in the same way as b_{11} and b_{12}, respectively, but horizontally not vertically. On the other hand, Fig. 2(c) shows the division of the constellation points according to the value of b_{21} being 1 or 0. For the second bit of U_2, b_{22}, the constellation diagram is divided in the same way as in Fig. 2(c) but horizontally not vertically.

Since Fig. 2 clearly divides the constellation into decision regions according to each bit, we will use it to derive the average BER expressions for both U_1 and U_2 using a set of decision thresholds denoted by λ_i which can be given as

$$\lambda_0 = 0, \quad \lambda_i = \frac{\delta_i + \delta_{i+1}}{2}, \forall i \in \{1, 2, 3\}, \tag{24}$$

where the values of the δ's are given as

$$\begin{aligned} &\delta_1 = h_1^{eff} - h_2^{eff}, \quad \delta_2 = h_1^{eff} + h_2^{eff}, \\ &\delta_3 = 3h_1^{eff} - h_2^{eff}, \quad \delta_4 = 3h_1^{eff} + h_2^{eff}. \end{aligned} \tag{25}$$

In the following BER calculations, we assume that $\delta_4 > \lambda_3 > \delta_3 > \lambda_2 > \delta_2 > \lambda_1 > \delta_1 > 0$. Although these values depend on the values of the effective channels, h_i^{eff}, which are RVs by nature, we derive all the BER expressions assuming this desired order. The rationale of this choice is driven by the fact that this order can be achieved with optimized uplink PA based on minimizing the obtained BER expressions. This uplink PA will ensure that the correct order is satisfied by reducing the channel ambiguity among the users, as it heavily penalizes the average BER cost function.

A. Analysis of U_1

To calculate the average BER of U_1, we need to calculate the average probability of detection error of its individual bits, $b_{1i}, \forall i \in \{1, \ldots, 4\}$, and take the average over these probabilities. Let us assume that the columns of the constellation diagrams in Fig. 2 are numbered from left to right as $C_1, \ldots, C_8$. Starting with b_{11}, a detection error can occur if any of the blue constellation points in Fig. 2(a) moves to the negative side of the real axis or if any of the red points moves to the positive side. For example, assuming that the true received constellation point belongs to the fifth column, C_5, and given h_i^{eff}, the conditional error probability of b_{11} can be expressed as

$$P_{b_{11}|h_i^{eff}, C_5} = \Pr\left(\mathfrak{Re}(n) < -\delta_1\right) = Q\left(\delta_1/\sigma_n\right), \tag{26}$$

where $Q(x) \triangleq \frac{1}{\sqrt{2\pi}} \int_x^{\infty} e^{-u^2/2} du$. Similarly, the conditional error probability of b_{11} can be calculated, given that the received constellation point belongs to any of the other columns, $C_m, \forall m$. Hence, the average bit error probability of b_{11}, averaged over all $C_m, \forall m \in \{1, \ldots, 8\}$, can be calculated as

$$P_{b_{11}|h_i^{eff}} = \frac{1}{4} \sum_{m=1}^{4} Q\left(\delta_m/\sigma_n\right). \tag{27}$$

On the other hand, we can notice from Fig. 2(b) that a detection error can occur in detecting the second bit of U_1, b_{12}, if any of the blue points exceeds the decision region bounds, that is, from $-\lambda_2$ to λ_2 on the real axis, or if any of the red points enters that region. Hence, to calculate the

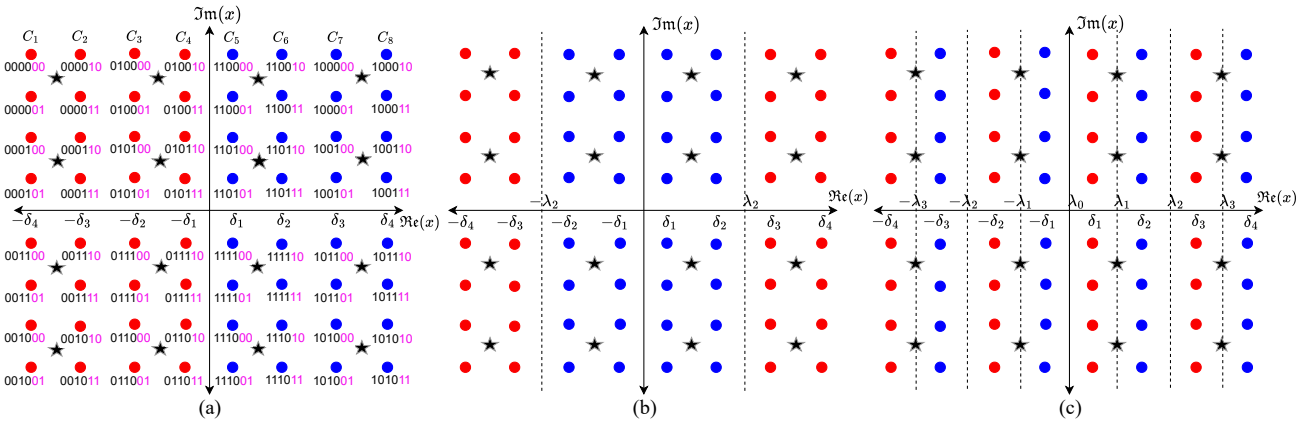

Figure 2: Combined uplink NOMA constellations for the two-user system employing 16-QAM for U_1 and 4-QAM for U_2: (a) b_{11}, (b) b_{12}, (c) b_{21}.

detection error probability of b_{12}, we calculate the conditional error probability given that the received constellation point belongs to each of the columns, and then we take the average over all possible columns.

Given that the true received constellation point belongs to C_1, the conditional error probability of detecting b_{12} can be calculated as

$$\begin{aligned} P_{b_{12}|h_i^{eff},C_1} &= \Pr\left(-\lambda_2+\delta_4 < \mathfrak{Re}(n) < \lambda_2+\delta_4\right) \\ &= Q\left(\frac{-\lambda_2+\delta_4}{\sigma_n}\right) - Q\left(\frac{\lambda_2+\delta_4}{\sigma_n}\right). \end{aligned} \tag{28}$$

Similarly, if the received constellation point belongs to C_m, the conditional error probability of detecting b_{12} can be calculated as

$$\begin{aligned} P_{b_{12}|h_i^{eff},C_m} &= \Pr\Big(\mathfrak{Re}(n) > (-1)^{\lceil \frac{m}{2} \rceil}\lambda_2 + \delta_{5-m}, \\ &\quad \mathfrak{Re}(n) < (-1)^{\lceil \frac{m}{2} \rceil+1}\lambda_2 + \delta_{5-m}\Big) \\ &= (-1)^{\lceil \frac{m}{2} \rceil} Q\left(\frac{\lambda_2 + (-1)^{\lceil \frac{m}{2} \rceil+1}\delta_{5-m}}{\sigma_n}\right) \\ &\quad + Q\left(\frac{(-1)^{\lceil \frac{m}{2} \rceil}\lambda_2 + \delta_{5-m}}{\sigma_n}\right), \quad \forall m \in \{1,2,3,4\}. \end{aligned} \tag{29}$$

Due to symmetry in Fig. 2(b), it is clear that the cases of C_5, C_6, C_7 and C_8 are similar to the cases of C_4, C_3, C_2 and C_1, respectively. Therefore, the average detection error probability of b_{12} can be obtained by averaging over the first four columns as

$$P_{b_{12}|h_i^{eff}} = \frac{1}{4}\sum_{m=1}^{4} P_{b_{12}|h_i^{eff},C_m}. \tag{30}$$

Finally, since b_{13} and b_{14} are similar to b_{11} and b_{12}, the conditional average BER of U_1 given the values of the effective channels, h_i^{eff}, can be calculated by taking the average of the error probabilities of b_{11} and b_{12} as

$$P_{U_1|h_i^{eff}} = 0.5(P_{b_{11}|h_i^{eff}} + P_{b_{12}|h_i^{eff}}), \tag{31}$$

where $P_{b_{11}|h_i^{eff}}$ and $P_{b_{12}|h_i^{eff}}$ are given in (27) and (30), respectively.

B. Analysis of U_2

To calculate the average BER of U_2, we need to calculate the probability of detection error of its two individual bits, b_{21} and b_{22}, then taking the average of them. Figure 2(c) shows the constellation mapping of b_{21}, where the blue points represent $b_{21}=1$ while the red points represent having $b_{21}=0$. The constellation mapping of b_{22} is exactly the same as shown in Fig. 2(c) but horizontally not vertically. Hence, b_{21} and b_{22} have similar detection error probabilities due to the symmetry of their constellation mappings, which makes the average BER of U_2 equal to the probability of detection error of b_{21}.

From Fig. 2(c), an error can occur when detecting b_{21} if any of the blue constellation points moves to the decision regions of the red points or vice versa. To calculate the total average detection error probability of b_{21}, we derive the conditional error probability given that the received constellation point belongs to C_i, then we take the average over all the possible 8 columns. However, due to the symmetry between the red columns and the blue columns in Fig. 2(c), we only calculate the conditional error probability given C_1, C_3, C_5 and C_7, and then we take the average over them.

Assuming that the true received constellation point belongs to C_1, and given h_i^{eff}, the conditional error probability of b_{21} can be expressed as

$$\begin{aligned} P_{b_{21}|h_i^{eff},C_1} &= \Pr\Big(\mathfrak{Re}(n) \in \{[-\lambda_3+\delta_4, -\lambda_2+\delta_4] \cup \\ &\quad [-\lambda_1+\delta_4, \delta_4] \cup [\lambda_1+\delta_4, \lambda_2+\delta_4] \cup [\lambda_3+\delta_4, \infty]\}\Big) \\ &= Q\left(\frac{-\lambda_3+\delta_4}{\sigma_n}\right) - Q\left(\frac{-\lambda_2+\delta_4}{\sigma_n}\right) + Q\left(\frac{-\lambda_1+\delta_4}{\sigma_n}\right) \\ &\quad - Q\left(\frac{\delta_4}{\sigma_n}\right) + Q\left(\frac{\lambda_1+\delta_4}{\sigma_n}\right) - Q\left(\frac{\lambda_2+\delta_4}{\sigma_n}\right) + Q\left(\frac{\lambda_3+\delta_4}{\sigma_n}\right). \end{aligned} \tag{32}$$

If the received constellation point belongs to C_3, the condi-

tional error probability of detecting b_{21} can be expressed as

$$\begin{aligned}P_{b_{21}|h_i^{eff},C_3} &= \Pr\Big(\mathfrak{Re}(n) \in \{[-\lambda_3+\delta_2, -\lambda_2+\delta_2] \cup \\ &\quad [-\lambda_1+\delta_2, \delta_2] \cup [\lambda_1+\delta_2, \lambda_2+\delta_2] \cup [\lambda_3+\delta_2, \infty]\}\Big) \\ &= Q\left(\frac{-\lambda_3+\delta_2}{\sigma_n}\right) - Q\left(\frac{-\lambda_2+\delta_2}{\sigma_n}\right) + Q\left(\frac{-\lambda_1+\delta_2}{\sigma_n}\right) \\ &\quad - Q\left(\frac{\delta_2}{\sigma_n}\right) + Q\left(\frac{\lambda_1+\delta_2}{\sigma_n}\right) - Q\left(\frac{\lambda_2+\delta_2}{\sigma_n}\right) + Q\left(\frac{\lambda_3+\delta_2}{\sigma_n}\right).\end{aligned} \tag{33}$$

In the case of receiving a constellation point that belongs to C_5, the conditional error probability of detecting b_{21} can be given as

$$\begin{aligned}P_{b_{21}|h_i^{eff},C_5} &= \Pr\Big(\mathfrak{Re}(n) \in \{[-\lambda_3-\delta_1, -\lambda_2-\delta_1] \cup \\ &\quad [-\lambda_1-\delta_1, -\delta_1] \cup [\lambda_1-\delta_1, \lambda_2-\delta_1] \cup [\lambda_3-\delta_1, \infty]\}\Big) \\ &= Q\left(\frac{-\lambda_3-\delta_1}{\sigma_n}\right) - Q\left(\frac{-\lambda_2-\delta_1}{\sigma_n}\right) + Q\left(\frac{-\lambda_1-\delta_1}{\sigma_n}\right) \\ &\quad - Q\left(\frac{-\delta_1}{\sigma_n}\right) + Q\left(\frac{\lambda_1-\delta_1}{\sigma_n}\right) - Q\left(\frac{\lambda_2-\delta_1}{\sigma_n}\right) + Q\left(\frac{\lambda_3-\delta_1}{\sigma_n}\right).\end{aligned} \tag{34}$$

When the received constellation point belongs to C_7, the conditional error probability of detecting b_{21} can be calculated as

$$\begin{aligned}P_{b_{21}|h_i^{eff},C_7} &= \Pr\Big(\mathfrak{Re}(n) \in \{[-\lambda_3-\delta_3, -\lambda_2-\delta_3] \cup \\ &\quad [-\lambda_1-\delta_3, -\delta_3] \cup [\lambda_1-\delta_3, \lambda_2-\delta_3] \cup [\lambda_3-\delta_3, \infty]\}\Big) \\ &= Q\left(\frac{-\lambda_3-\delta_3}{\sigma_n}\right) - Q\left(\frac{-\lambda_2-\delta_3}{\sigma_n}\right) + Q\left(\frac{-\lambda_1-\delta_3}{\sigma_n}\right) \\ &\quad - Q\left(\frac{-\delta_3}{\sigma_n}\right) + Q\left(\frac{\lambda_1-\delta_3}{\sigma_n}\right) - Q\left(\frac{\lambda_2-\delta_3}{\sigma_n}\right) + Q\left(\frac{\lambda_3-\delta_3}{\sigma_n}\right).\end{aligned} \tag{35}$$

Thus, the average BER of U_2 given the effective channels, h_i^{eff}, can be calculated as

$$P_{U_2|h_i^{eff}} = P_{b_{21}|h_i^{eff}} = \frac{1}{4}\sum_{m=0}^{3} P_{b_{21}|h_i^{eff},C_{2m+1}}, \tag{36}$$

where $P_{b_{21}|h_i^{eff},C_{2m+1}}$ for $m = 0, 1, 2$, and 3 is given in (32), (33), (34), and (35), respectively.

After deriving the conditional BERs given the instantaneous effective channels of the users, the derivation of the average unconditional BER expressions of U_1 and U_2 is presented in Sec. V-B. This is performed by averaging the expressions obtained in (31) and (36), respectively, over the probability density functions (PDFs) of the effective channels, h_1^{eff} and h_2^{eff}.

V. Design and BER analysis of the generalized K-user M-QAM uplink RIS-NOMA system

In this section, a framework is presented for deriving closed-form BER expressions for the generalized uplink RIS-NOMA system with an arbitrary number of users and arbitrary QAM modulation orders. Specifically, we extend our BER analysis to the generalized system by specifically providing an algorithm that calculates the coefficients of the BER expressions for an arbitrary number of users and QAM modulation orders. Then, we provide a methodology to derive the unconditional average BER expressions of the generalized system by averaging over the CFs of the effective channels of the K users.

A. Generalization for arbitrary number of users and QAM modulation orders

In this subsection, we generalize our analysis by devising a methodology to obtain the BER expressions for a general uplink RIS-NOMA system with arbitrary number of users and arbitrary QAM modulation orders for the users. From Sec. IV, we have found that the conditional BER expressions always take the form of a weighted sum of $Q(\cdot)$ functions having different linear combinations of the effective channels, h_i^{eff}, as arguments. Consequently, for a general K-user system, the conditional BER expression of user k, given the effective channel values, $h_i^{eff}, \forall i$, can be expressed as

$$BER_{U_k|h_1^{eff},\ldots,h_K^{eff}} = \sum_{q=1}^{N_k} c_{k,q} Q\left(\frac{\sum_{i=1}^{K} a_{k,iq} h_i^{eff}}{\sigma_n}\right), \tag{37}$$

where N_k is the total number of $Q(\cdot)$ functions in the BER expression of U_k, while the coefficients $c_{k,q}$ and $a_{k,iq}$ depend on the number of users, K, and the QAM modulation orders used by these users. Therefore, by devising an algorithm that can compute these coefficients for arbitrary number of users and QAM modulation orders, we can calculate the conditional BER expressions for a generalized uplink RIS-NOMA system.

Due to applying the proposed channel alignment scheme in Sec. III-B, the received superimposed uplink NOMA constellation at the BS is constructed as the constellation of downlink NOMA systems. Therefore, utilizing the proposed channel alignment scheme allows us to use the methodology provided in Sec. III of [41] for deriving the generalized BER expressions of downlink NOMA systems. Section III of [41] provides a methodology to obtain the weights of the $Q(\cdot)$ functions, $c_{k,q}$, in (37), but does not calculate the coefficients, $a_{k,iq}$, which are inside the $Q(\cdot)$ functions. The reason for this is that, unlike uplink NOMA systems, the constellation of downlink NOMA systems experiences only one fading channel before reception at the user, where the signal received at the kth user can be given as

$$y_k = \left(\sum\nolimits_{i=1}^{K} \sqrt{\rho_i} x_i\right) h_k + n_k, \tag{38}$$

where ρ_i is the power allocated to user i, while h_k and n_k are the fading channel and additive white Gaussian noise (AWGN) of the kth user, respectively. However, the methodology in [41] calculates the error distances of the downlink NOMA constellation which can be written as

$$\Delta_{k,q} = \sum\nolimits_{i=1}^{K} a_{k,iq} \sqrt{\rho_i}, \tag{39}$$

where $a_{k,iq}, \forall i, q$ are the required coefficients for the kth user in (37). Hence, setting ρ_i to some known values, we can compute the coefficients, $a_{k,iq}$, of the kth user by knowing the

distances, $\Delta_{k,q}$, using **Algorithm 1**. The ith element of the input vector, $\mathbf{b}$, of **Algorithm 1** is the number of bits per symbol of the ith user, b_i, representing its modulation order, while $\boldsymbol{\rho}$ contains the power coefficients of the users, $\rho_i, \forall i$. The vector, $\boldsymbol{\Delta}_k$, contains all the error distances of the kth user, $\Delta_{k,q}, \forall q$. The output of **Algorithm 1** are the matrices, $\mathbf{A}_1, \ldots, \mathbf{A}_K$, which contain the required coefficients, $a_{k,iq}, \forall i, q$, that is, the element of the qth row and the ith column of $\mathbf{A}_k$ is $a_{k,iq}$.

Algorithm 1: Calculation of $a_{k,iq}, \forall k, i, q$.

Inputs: $\mathbf{b}$ and $\boldsymbol{\rho}$.
for *k=1:K* **do**
  Calculate $\boldsymbol{\Delta}_k^{(1)}$ using the method in [41], with inputs $\mathbf{b}$ and $\boldsymbol{\rho}$.
  for $i = 1 : K$ **do**
    Set ε to any small value, e.g., $\varepsilon = 0.1$;
    Set $\boldsymbol{\rho}' = \boldsymbol{\rho}$;
    Set $\boldsymbol{\rho}'(i) = \left(\sqrt{\boldsymbol{\rho}(i)} + \varepsilon\right)^2$;
    Calculate $\boldsymbol{\Delta}_k^{(2)}$ using the method in [41], with inputs $\mathbf{b}$ and $\boldsymbol{\rho}'$.
    for $q = 1 : \text{length}\left(\boldsymbol{\Delta}_k^{(1)}\right)$ **do**
      $\mathbf{A}_k(q, i) = \frac{\boldsymbol{\Delta}_k^{(2)}(q) - \boldsymbol{\Delta}_k^{(1)}(q)}{\varepsilon}$;
    end
  end
end
Return: $\mathbf{A}_1, \mathbf{A}_2, \ldots, \mathbf{A}_K$.

The idea of **Algorithm 1** is that the coefficient, a_{iq}, in (39) can be calculated using the partial differentiation of $\Delta_{k,q}$ with respect to (w.r.t.) $\sqrt{\rho_i}$. Since $\Delta_{k,q}$ is a linear function in $\sqrt{\rho_i}$, then the partial derivative of $\Delta_{k,q}$ w.r.t. $\sqrt{\rho_i}$ can be calculated as

$$a_{k,iq} = \mathbf{A}_k(q, i) = \frac{\partial \Delta_{k,q}}{\partial \sqrt{\rho_i}} = \frac{\Delta_{k,q}^{(2)} - \Delta_{k,q}^{(1)}}{\sqrt{\rho_i}^{(2)} - \sqrt{\rho_i}^{(1)}}, \quad \forall k, i, q. \tag{40}$$

The power coefficients, ρ_i, are set in **Algorithm 1** as $\rho_i = 2^{\sum_{i+1}^{K} b_i}, \forall i < K$ and $\rho_K = 1$, because this setting prevents overlapping between the superimposed NOMA constellation points.

B. Averaging the BER expressions over the PDFs of the RIS effective channels

In this subsection, we average the obtained conditional BER expressions in (37) over the PDFs of $h_i^{eff}, \forall i$. The argument inside the qth $Q(\cdot)$ function of the BER expression of the kth user can always be expressed as

$$X_{k,q} = \sum\nolimits_{i=1}^{K} a_{k,iq} h_i^{eff}. \tag{41}$$

Therefore, the CF of $X_{k,q}$ can be given as

$$\Phi_{X_{k,q}}(z) = \prod\nolimits_{i=1}^{K} \Phi_{h_i^{eff}}(a_{k,iq} z), \tag{42}$$

where $\Phi_{h_i^{eff}}(z)$ is given in (22). Finally, Proposition 1 gives the final unconditional BER of U_k.

Proposition 1. *By averaging (37) over the statistical distributions of $h_i^{eff}, \forall i$, the unconditional average BER of U_k can be given as*

$$BER_{U_k} = \sum_{q=1}^{N_k} \frac{c_{k,q}}{2} + \frac{c_{k,q}}{\pi} \int_0^{\infty} \mathfrak{Re}\left(\frac{j' e^{\frac{-z^2}{2}}}{z} \Phi_{X_{k,q}}\left(\frac{z}{\sigma_n}\right) \right) dz.$$

Proof. See Appendix A. ∎

VI. Extending the analysis to the imperfect CSI case

In practical systems, the cascaded RIS channel vector of the ith user, $\mathbf{r}_{ii} \triangleq \mathbf{h}_{ii} \odot \mathbf{g}_i$, where $\odot$ is the Hadamard product, is estimated at the BS using the linear minimum mean square error estimator (LMMSE) technique [42]. The channel estimate at the BS can be expressed as

$$\widehat{\mathbf{r}}_{ii} = \overline{\mathbf{r}}_{ii} + \widehat{\mathbf{r}}_{ii}^{\text{zero}}, \tag{43}$$

where $\overline{\mathbf{r}}_{ii} = \mathbb{E}(\mathbf{r}_{ii}) = \sqrt{K_1 K_2 / (K_1+1)(K_2+1)} \mathbf{h}_{ii}^{LoS} \odot \mathbf{g}_i^{LoS}$ is the constant mean vector, while $\widehat{\mathbf{r}}_{ii}^{\text{zero}}$ is the estimate of the random zero mean part, $\mathbf{r}_{ii}^{\text{zero}}$; $\overline{\mathbf{r}}_{ii}$ is typically assumed to be known previously at the BS as it changes at a much lower pace than the random component $\mathbf{r}_{ii}^{\text{zero}}$. The estimation error model that is commonly used to model the impact of imperfect CSI is given as [43], [44]

$$\mathbf{r}_{ii}^{\text{zero}} = \widehat{\mathbf{r}}_{ii}^{\text{zero}} + \boldsymbol{\Delta}\mathbf{r}_{ii}^{\text{zero}}, \tag{44}$$

where $\boldsymbol{\Delta}\mathbf{r}_{ii}^{\text{zero}} \in \mathbb{C}^{L_i \times 1}$ represents the estimation error vector whose lth element, $\Delta r_{ii,l}^{\text{zero}}$, is orthogonal to the lth element of $\widehat{\mathbf{r}}_{ii}^{\text{zero}}$, i.e., $\Delta r_{ii,l}^{\text{zero}}$ and $\widehat{r}_{ii,l}^{\text{zero}}$ are mutually uncorrelated. The variance of the MMSE estimates is equal to $\text{Var}(\widehat{r}_{ii,l}^{\text{zero}}) = \omega^2 \varrho^2$, while $\text{Var}(\Delta r_{ii,l}^{\text{zero}}) = (1-\omega^2)\varrho^2$, where ω is the correlation coefficient between $\widehat{r}_{ii,l}^{\text{zero}}$ and $r_{ii,l}^{\text{zero}}$ and $\varrho^2 = \frac{K_1+K_2+1}{(K_1+1)(K_2+1)}$ is the variance of $r_{ii,l}^{\text{zero}}$.

Thus, the optimized component of the effective channel of user i can be given as

$$\begin{aligned} \gamma_{ii} &= u_i \boldsymbol{\theta}_i^T (\overline{\mathbf{r}}_{ii} + \mathbf{r}_{ii}^{\text{zero}}) = u_i \boldsymbol{\theta}_i^T (\overline{\mathbf{r}}_{ii} + \widehat{\mathbf{r}}_{ii}^{\text{zero}} + \boldsymbol{\Delta}\mathbf{r}_{ii}^{\text{zero}}) \\ &= u_i \boldsymbol{\theta}_i^T \widehat{\mathbf{r}}_{ii} + u_i \boldsymbol{\theta}_i^T \boldsymbol{\Delta}\mathbf{r}_{ii}^{\text{zero}} = \widehat{\gamma}_{ii} + u_i \boldsymbol{\theta}_i^T \boldsymbol{\Delta}\mathbf{r}_{ii}^{\text{zero}}, \end{aligned} \tag{45}$$

where $u_i = \sqrt{P_i \eta_i / \beta_i}$ and $\boldsymbol{\theta}_i = [e^{j'\theta_{i,1}}, \ldots, e^{j'\theta_{i,L_i}}]^T$ is the reflection coefficients vector of the ith partition $\mathcal{P}_i$ of the RIS. Since $\boldsymbol{\theta}_i$ is adjusted to cancel the phase of the estimated cascaded channel, $\widehat{\mathbf{r}}_{ii}$, then $\widehat{\gamma}_{ii} = u_i \sum_{l=1}^{L_i} |\widehat{r}_{ii,l}|$, where $\widehat{r}_{ii,l}$ is the lth element of $\widehat{\mathbf{r}}_{ii}$.

Now, we derive the mean and variance of $\widehat{\gamma}_{ii}$. The cascaded channel estimate $\widehat{r}_{ii,l}$ is an affine function of the observation $r_{ii,l}^{\text{obs}} = r_{ii,l} + w$, in the case of LMMSE, where w is added complex Gaussian noise. Since $r_{ii,l}$ is a product of two non-central complex Gaussian RVs, we can employ the complex normal distribution to approximate $\widehat{r}_{ii,l}$. Therefore, $|\widehat{r}_{ii,l}|$ follows the Ricean distribution having an amplitude of the deterministic component of $\widehat{\nu}_{ii} = \sqrt{K_1 K_2 / (K_1+1)(K_2+1)}$ and a total variance of the random component, $\widehat{r}_{ii,l}^{\text{zero}}$, of $2\widehat{\sigma}_{ii,l}^2$, where $\widehat{\sigma}_{ii,l}^2 = \omega^2 \varrho^2 / 2$. Therefore, $\mathbb{E}(|\widehat{r}_{ii,l}|)$ can be given as in (8) using the formulas for $\widehat{\nu}_{ii}$ and $\widehat{\sigma}_{ii,l}^2$, while the variance can be given as $\text{Var}(|\widehat{r}_{ii,l}|) = \widehat{\nu}_{ii}^2 + 2\widehat{\sigma}_{ii,l}^2 - \mathbb{E}(|\widehat{r}_{ii,l}|)^2$. Thus, the mean and variance of $\widehat{\gamma}_{ii}$ can be given as $\mathbb{E}(\widehat{\gamma}_{ii}) = \sqrt{P_i \eta_i / \beta_i} L_i \mathbb{E}(|\widehat{r}_{ii,l}|)$

and $\mathrm{Var}(\widehat{\gamma}_{ii})=^{P_i\eta_i}/_{\beta_i}L_i\mathrm{Var}(|\widehat{r}_{ii,l}|)$, where we can substitute these parameters in (11) and (12) to get the scale and shape parameters of $\widehat{\gamma}_{ii}$ and hence the CF of the its Gamma fit, $\Phi_{\widehat{\gamma}_{ii}}(z)$.

Since γ_{ij} is estimated with only one single pilot signal, its estimation complexity (and error) are negligible compared to γ_{ii} as it does not scale with the size of the RIS. Hence, we can relatively accurately assume perfect knowledge of γ_{ij}. Therefore, the estimated effective channel of user i after applying the channel alignment scheme in Sec. III-B can be given as

$$\widehat{h}_i^{eff} \approx \widehat{\gamma}_{ii} + \sum\nolimits_{j=1,j\neq i}^{K} \mathfrak{Re}(\gamma_{ij}). \tag{46}$$

The received signal at the BS can then be written as

$$y = \underbrace{\sum\nolimits_{i=1}^{K} \widehat{h}_i^{eff} x_i}_{\text{Data over estimated ch.}} + \underbrace{\sum\nolimits_{i=1}^{K} \sqrt{P_i\eta_i/\beta_i}\boldsymbol{\theta}_i^T \boldsymbol{\Delta}\mathbf{r}_{ii}^{\text{zero}} x_i}_{\text{Data over unknown ch.}} + n. \tag{47}$$

In (47), the data symbols are received in two directions, the estimated effective channel and the unknown channel. The received data over the unknown channel is ambiguous and cannot be detected successfully and therefore can be treated as self-interference at the BS. Since the power of this self-interference depends on the magnitude data symbols, x_i, which vary according to the transmitted data symbols from the QAM constellation, the BER can be upper bounded by substituting the highest magnitude data symbols in the interference power. Thus, the interference power can be given as $\sigma_{Int}^2=\sum_{i=1}^{K} P_i\eta_i/\beta_i L_i|x_i^{\max}|^2(1-\omega^2)\varrho^2$ and it can be modeled as Gaussian interference with zero mean according to CLT. Finally, the BER of U_i can be upper bounded using the same expression as in Proposition 1 by replacing σ_n with $\sqrt{\sigma_{Int}^2+\sigma_n^2}$ and $\Phi_{\gamma_{ii}}(z)$ with $\Phi_{\widehat{\gamma}_{ii}}(z)$.

VII. Extending the uplink RIS-NOMA design to the multi-antenna BS case

When the BS have multiple antennas, optimized receive combiners, $\mathbf{w}_k \forall k$, for the users, shall be designed to further utilize the receive diversity effect. The received signal vector at the BS in an N-antenna BS scenario can be given as

$$\mathbf{y} = \sum\nolimits_{i=1}^{K} \sqrt{P_i\eta_i/\beta_i}\left(\left(\sum\nolimits_{j=1}^{K} \mathbf{G}_j^T\boldsymbol{\Theta}_j\mathbf{h}_{ij}\right) + \mathbf{v}_i\right) x_i + \mathbf{n}, \tag{48}$$

where $\mathbf{G}_i \in \mathbb{C}^{L_i\times N}$ is the channel matrix between the ith portion of the RIS, $\mathcal{P}_i$, and the BS, and follows the Ricean fading model with parameter K_2. The vector $\mathbf{v}_i$ is the direct Rayleigh fading channel from U_i to the BS, while $\mathbf{n}$ is the AWGN noise vector at the BS. The received signal vector, $\mathbf{y}$, is multiplied at the BS by a receive combiner, $\mathbf{w}\in\mathbb{C}^{N\times 1}$, to project $\mathbf{y}$ on the direction that maximizes the desired signal strength. However, $\mathbf{w}$ designed and optimized jointly with $\boldsymbol{\Theta}$, as we show below.

The receiving antennas at the BS are divided among the users as in the case of the RIS, so that each antenna subgroup is responsible for projecting the signal of U_i. In this case, $\mathbf{w}$ is subdivided into K sub-vectors as $\mathbf{w}=[\mathbf{w}_1^T,\ldots,\mathbf{w}_K^T]^T$, where $\mathbf{w}_i$ is the receiving combiner of U_i. The sub-vector, $\mathbf{w}_i$, is jointly optimized with $\boldsymbol{\Theta}_i$ to maximize the received amplitude of U_i's signal as

$$\max_{\boldsymbol{\Theta}_i,\mathbf{w}_i} \quad |\mathbf{w}_i^T(\mathbf{G}_{ii}^T\boldsymbol{\Theta}_i\mathbf{h}_{ii} + \mathbf{v}_{ii})| \tag{49a}$$

$$\text{s.t.} \quad 0 \le \theta_{i,l} \le 2\pi,\ \forall l, \quad \|\mathbf{w}_i\| = 1,\ \forall i, \tag{49b}$$

where $\mathbf{G}_{ii}$ is the channel matrix between $\mathcal{P}_i$ and the antenna subgroup of U_i at the BS, and $\mathbf{v}_{ii}$ is the direct channel vector from U_i to its associated antenna subgroup. Although being non-convex, (49) can be efficiently solved using block coordinate descent (BCD) by alternatively fixing one of the optimization vectors and solving for the other until convergence is reached. For a fixed $\mathbf{w}_i$, the subproblem in $\boldsymbol{\Theta}_i$ has a closed-form optimal solution by exploiting the special structure of its objective function in (49a), which is given as

$$\theta_l^\star = \arg(\mathbf{w}_i^T\mathbf{v}_{ii}) - \arg(h_{ii,l}) - \arg(\mathbf{w}_i^T\mathbf{g}_{ii,l}), \tag{50}$$

where $\mathbf{g}_{ii,l}$ is the lth column of $\mathbf{G}_{ii}^T$. On the other hand, for fixed $\boldsymbol{\Theta}_i$, the optimal $\mathbf{w}_i^\star$ that maximizes (49a) also has a closed-form solution, which is maximum ratio combining (MRC), i.e., $\mathbf{w}_i^\star=\frac{(\mathbf{G}_{ii}^T\boldsymbol{\Theta}_i\mathbf{h}_{ii}+\mathbf{v}_{ii})^*}{\|\mathbf{G}_{ii}^T\boldsymbol{\Theta}_i\mathbf{h}_{ii}+\mathbf{v}_{ii}\|}$. The above alternating optimization approach is practically appealing since both the receive combiner and phase shifts are obtained in closed-form expressions, which is a significantly low-complexity solution.

The received signal vector, $\mathbf{y}$, is then multiplied by the receive combiner, $\mathbf{w}$, thus the final superimposed NOMA signal can be written as

$$y = \sum_{i=1}^{K}\sqrt{\frac{P_i\eta_i}{\beta_i}}\sum_{k=1}^{K}\mathbf{w}_k^T\left(\sum_{j=1}^{K}\mathbf{G}_{jk}^T\boldsymbol{\Theta}_j\mathbf{h}_{ij} + \mathbf{v}_{ik}\right)x_i + \widetilde{n}, \tag{51}$$

where $\widetilde{n} = \mathbf{w}^T\mathbf{n}$. Therefore, the effective channel component of U_i that is reflected by $\mathcal{P}_i$ is given as

$$\gamma_{ii} = \underbrace{\mathbf{w}_i^{\star T}(\mathbf{G}_{ii}^T\boldsymbol{\Theta}_i^\star\mathbf{h}_{ii} + \mathbf{v}_{ii})}_{\gamma_{ii}^{opt}} + \underbrace{\sum_{\substack{k=1\\k\neq i}}^{K}\mathbf{w}_k^T(\mathbf{G}_{ik}^T\boldsymbol{\Theta}_i^\star\mathbf{h}_{ii} + \mathbf{v}_{ik})}_{\gamma_{ii}^{rand}}, \tag{52}$$

where γ_{ii}^{opt} is the optimized component since $\mathbf{w}_i^\star$ and $\boldsymbol{\Theta}_i^\star$ are optimized only for $\mathbf{G}_{ii}$, while γ_{ii}^{rand} is a random residual component. The random channel component of U_i reflected by $\mathcal{P}_j$ can be expressed as

$$\gamma_{ij} = \sum\nolimits_{k=1}^{K}\mathbf{w}_k^T\left(\sum\nolimits_{j=1}^{K}\mathbf{G}_{jk}^T\boldsymbol{\Theta}_j\mathbf{h}_{ij} + \mathbf{v}_{ik}\right). \tag{53}$$

Thus, by applying the channel alignment scheme in Sec. III-B, the final effective channel of U_i can be given as

$$h_i^{eff} \approx \gamma_{ii}^{opt} + \gamma_{ii}^{rand} + \sum\nolimits_{j=1,j\neq i}^{K}\mathfrak{Re}(\gamma_{ij}). \tag{54}$$

γ_{ii}^{opt} is always a positive RV and therefore can be modeled as a Gamma RV, while the other two terms in (54) can be modeled as Gaussian RVs. However, obtaining mathematical formulas for the means and variances of these RVs is not tractable due to the iterative optimization process involved in (49). Thus, the first and second moments of the Gamma and Gaussian RVs shall be calculated empirically and used to calculate the parameters of the corresponding CFs. Finally, the BER of U_i

can be given as the same expression as in Proposition 1, using the new obtained CFs of the multi-antenna case.

VIII. Average BER minimization-based power allocation scheme

In this section, we introduce an optimized uplink PA scheme for the RIS-NOMA system. The aim of this PA is to eliminate the BER floors that occur in SIC-based uplink NOMA systems. Specifically, the transmit powers of the users are optimized to minimize the overall average BER performance at the BS for all users while adhering to individual uplink transmit power constraints. The optimization process is clearer and more robust when conducted in the log-log domain, where both the power values to be optimized, P_k, and the cost function are expressed in dB. This transformation results in smoother numerical optimization and faster convergence when applying gradient descent-based optimization techniques to solve our problem. Therefore, the uplink PA problem can be formulated as

$$\min_{P_1,\ldots,P_K} 10\log_{10}\left(\sum\nolimits_{k=1}^{K} BER_{U_k}\left(10^{\frac{P_1}{10}},\ldots,10^{\frac{P_K}{10}}\right)\right) \quad (55a)$$

$$\text{s.t.} \quad P_k \leq P_{\mathrm{dBm}}^{\max}, \qquad \forall k, \quad (55b)$$

where $P_{\mathrm{dBm}}^{\max}$ represents the maximum available uplink transmit power in dBm, and BER_{U_k} in (55a) is the general BER formula of U_k given in Proposition 1.

We use a gradient-based method to solve (55) where the cost function along with the constraints are all continuous and have continuous first derivatives. To deal with the constraints, we shall transform (55) into an unconstrained optimization problem by constructing the Lagrangian that is given as

$$L(\mathbf{p},\xi_1,\ldots,\xi_K) = f(\mathbf{p}) + \sum\nolimits_{k=1}^{K} \xi_k(P_k - P_{dBm}^{\max}), \quad (56)$$

where ξ_k is the Lagrange multiplier that corresponds to the kth constraint, f is the cost function in (55), and $\mathbf{p} = [P_1,\ldots,P_K]^T$. The Lagrangian in (56) is optimized using Newton's gradient-based method, utilizing the Hessian operator of the Lagrangian. Given that the constraints are linear functions, the Hessian in this case only includes the Hessian of the original objective function f, as it represents the second derivative of L. Therefore, the Hessian of L can be given as

$$\nabla^2 L = \nabla^2 f(\mathbf{p}), \quad (57)$$

where ∇^2 is the Laplacian operator or the second order differential operator. Newton's method is an iterative algorithm that is applied using a starting point $\mathbf{p}_0$ in an iterative manner until convergence to the optimum point. The update rule in each iteration can be given as

$$\mathbf{p}_{n+1} = \mathbf{p}_n - \left[\nabla^2 f(\mathbf{p}_n)\right]^{-1} \nabla f(\mathbf{p}_n). \quad (58)$$

The Lagrange multipliers, ξ_k, in (56) are hyperparameters that are adjusted iteratively until convergence is reached. This involves repeatedly optimizing the Lagrangian, starting with initial values for ξ_k, which are updated in each iteration. Generally, we start with high values for ξ_k and modify them based on how much the constraints are satisfied in every iteration. If $(P_k - P_{dBm}^{\max}) < 0$, the corresponding Lagrange multiplier, ξ_k, should be decreased. Conversely, if $(P_k - P_{dBm}^{\max}) > 0$, indicating a constraint violation, ξ_k should be increased.

It is important to highlight that while the optimization process described above is iterative, it relies on the average channel statistics of the users rather than their instantaneous channel coefficients. This aspect simplifies the hardware implementation of the PA algorithm. Specifically, the PA problem outlined in (55) is defined solely by the users' channel variances, σ_k^2, and the average received noise power, σ_n^2, all of which exhibit long coherence times. This method ensures that the proposed PA strategy remains computationally efficient while providing minimized average BER performance for all NOMA users, making it suitable for real-world applications.

IX. Simulation Results

In this section, we provide simulation results for the achievable BER of the introduced system under different operating conditions. We also validate our derived expressions using Monte-Carlo simulations. The BER performance of the users is plotted against the transmit power.

We adopt similar simulation parameters to those used in [10] and [45], which can be summarized as follows. The path loss exponent of the RIS channels is $\psi = 2.2$, while the path loss exponent of the direct links (users to BS) is $\psi^{\mathrm{dir}} = 4$. The noise power in the real or imaginary dimensions, σ_n^2, is set to be -90 dBm, and the Ricean factors in (2) and (3) are set as $K_1 = K_2 = 2.2$.

Moreover, the achievable BER performance of the RIS-NOMA system is compared to the RIS-OMA counterpart that applies time division multiple access (TDMA). For fair comparison, the time slot allocated to a certain user in RIS-TDMA-OMA scenario, T_{OMA}, equals the time slot in RIS-NOMA, T_{NOMA}, divided by the total number of users, K, i.e., $T_{\mathrm{NOMA}} = KT_{\mathrm{OMA}}$. In addition, we fix the achievable data rate for all users by making the total number of bits transmitted by each user during T_{OMA} equal to the total number of bits transmitted by that user during T_{NOMA}. By way of explanation, the modulation order for user k in RIS-TDMA-OMA equals its modulation order in RIS-NOMA scenario raised to power K, which guarantees that the total number of transmitted bits in both systems is equal for the same amount of consumed network resources. To achieve a fair comparison, only one partition is assigned to a certain user during its signaling time in the OMA benchmark, which is similar to the assignment when NOMA signaling is applied. This makes the OMA benchmark require the same number of channel estimates and RIS phase compensations as the NOMA scenario.

Figure 3 shows the BER performance of a two-user uplink RIS-NOMA system model against the transmission power of each user. The two users, U_1 and U_2, employ QAM with orders of 16 and 4 in NOMA signaling, while they use modulation orders of 256 and 16, respectively, when TDMA-OMA is applied. Moreover, the users' distances to the RIS are 20 m and 70 m, respectively, while the RIS-BS distance is 30 m. The elevation angles, Ω, of the users to the RIS are 140° and 110°, while the azimuth angles, Ψ, are 100° and 110°,

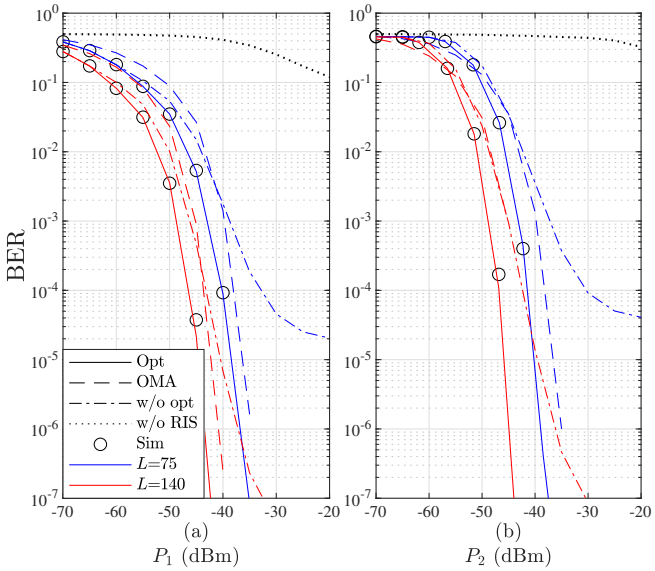

Figure 3: BER performance comparison between a two-user RIS-NOMA system and the RIS-OMA counterpart under different L values and $d_{U_1,I} = 20$, $d_{U_2,I} = 70$, $d_{I,B} = 30$: (a) U_1 (16-QAM), (b) U_2 (4-QAM).

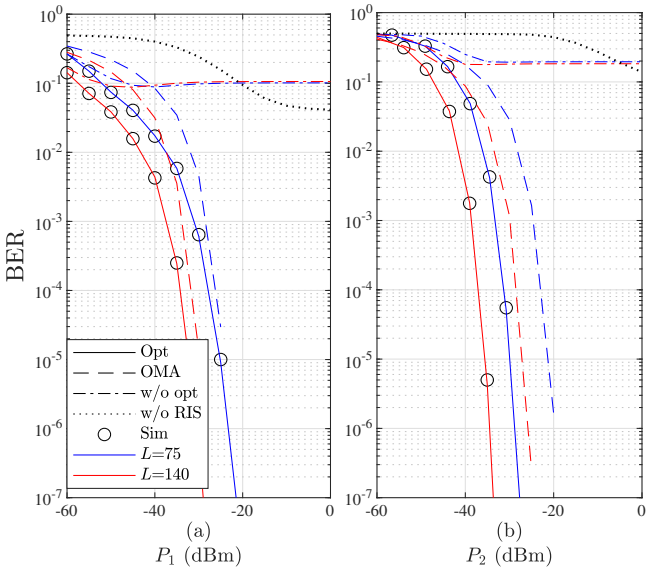

Figure 4: BER performance comparison between a two-user RIS-NOMA system and the RIS-OMA counterpart under different L values and $d_{U_1,I} = 20$, $d_{U_2,I} = 100$: (a) U_1 (64-QAM), (b) U_2 (16-QAM).

respectively. The figure also compares the RIS-NOMA with RIS-TDMA-OMA under two values for the number of RIS reflectors per user. In the first case, a number of $L_i = 75$ reflectors is assigned to each user, while $L_i = 140$ reflectors are assigned to each user in the second case. As can be seen in the figure, without optimization (w/o opt), the RIS-NOMA system suffers from a significant error floor which increases as L decreases. For example, the BER floor of the users is around 5×10^{-5} when $L_i = 70$. This error floor is attributed to the inter-user interference that dominates the AWGN at high SNR values. This error floor decreases when the number of RIS elements per user increases due to the signal-to-interference-plus-noise-ratio (SINR) enhancement gained by increasing L_i. However, as can be observed from the figure, the proposed PA algorithm in Sec. VIII has managed to eliminate the error floor by controlling the transmit power of each user, which in turn controls the amount of interference imposed by each user on other users. It can also be observed in Fig. 3 that NOMA outperforms TDMA-OMA for the whole range of SNR for the two users. Figure 3 also shows the severe performance inferiority of the system without employing RIS and relying only on direct links. There are two reasons for this; the first reason is the high path loss of direct links due to the harsh propagation environment, while the second is the high error floors that are nature in SIC based uplink NOMA systems. Finally, the figure shows a perfect match between the simulation results and the derived closed-form expressions, which confirms the accuracy of the analysis carried out in this paper.

Figure 4 shows the achievable BER for the same simulation parameters as Fig. 3, except for the modulation orders which have been increased to 64 and 16 in the NOMA scenario, and 2^{12} and 2^8 in the TDMA-OMA scenario, for U_1 and U_2, respectively. The distance of U_2 to the RIS is also increased to 100 m to provide a greater path loss difference between the two users as the modulation orders increased. As can be observed in Fig. 4, as the modulation orders increase, the BER performance suffers from extremely high error floors, which are around 10^{-1}, without applying the proposed PA scheme in Sec. VIII. On the other hand, the proposed PA scheme manages to completely remove the BER floors. It can also be clearly seen in Fig. 4 that optimized NOMA outperforms the TDMA-OMA counterpart for both users and for the entire range of SNR. Moreover, Fig. 4 shows the huge performance gain of the RIS aided scenario over the system without using RIS. Finally, the figure also confirms the analytical BER expressions derived in this paper.

To verify the analysis of the generalized case with multiple users, in Fig. 5, we present the achievable BER performance of a three-user uplink RIS-NOMA scenario. The simulation parameters for U_1 and U_2 remain the same as in Fig. 4, except for the number of reflectors considered in the simulation setup where $L = \{75, 150, 225\}$. The newly added U_3 employs 16-QAM and is located at 500 m from the RIS location. As can be observed from the figure, there is a perfect match between theoretical results and simulation for the three-user scenario, which confirms the derivations carried out in this paper. The figure also shows that the system's performance suffers from extremely high error floors at the level 10^{-1}, without applying the proposed PA scheme, while the error floor can be mitigated by using the proposed PA algorithm. This in turn gives clear superiority to the optimized NOMA system over TDMA-OMA for all users and for almost the entire operating SNR range.

Figure 6 examines three different optimization strategies for the uplink RIS-NOMA system when $L = 70$. The first strategy is the proposed PA scheme in Sec. VIII, while the second one (Element split) is based on optimizing L_1 and $L_2 = L - L_1$ by minimizing the average BER using

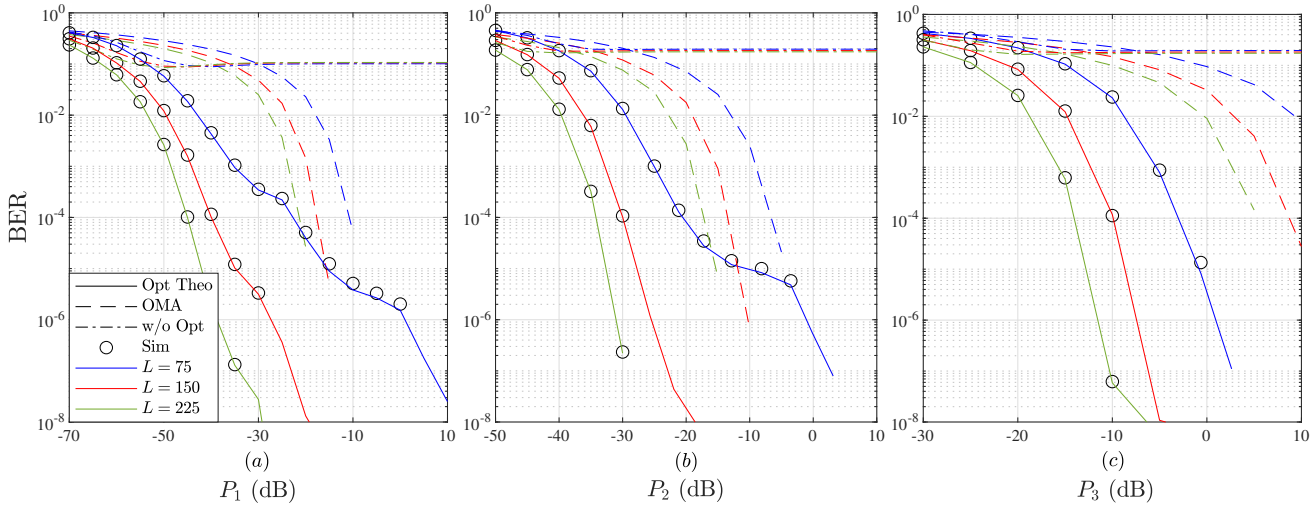

Figure 5: BER performance comparison between a three-user RIS-NOMA system and the RIS-OMA counterpart under different L values and $d_{U_1,I} = 20$, $d_{U_2,I} = 100$, $d_{U_3,I} = 500$: (a) U_1 (64-QAM), (b) U_2 (16-QAM), (c) U_3 (16-QAM).

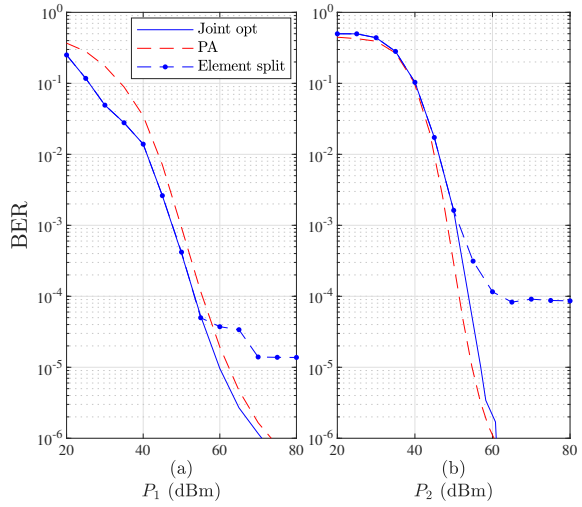

Figure 6: Comparison between different optimization strategies of a 4-QAM two-user uplink RIS-NOMA system ($L = 70$, $d_{U_1,I} = 20$, $d_{U_2,I} = 40$ m): (a) U_1, (b) U_2.

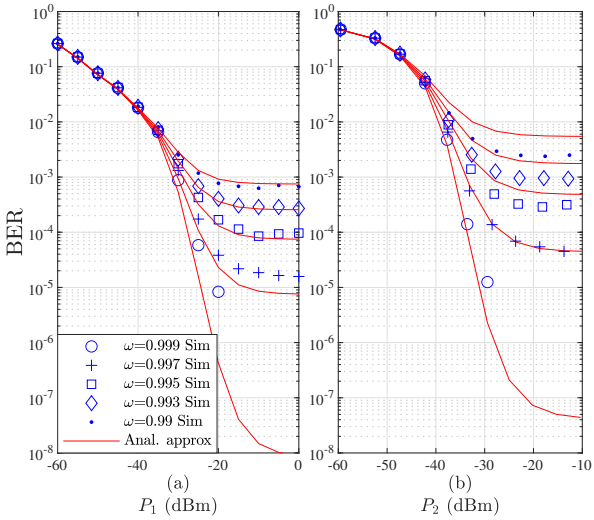

Figure 7: BER performance of a two-user RIS-NOMA system with imperfect CSI under different ω values and $L = 75$, $d_{U_1,I} = 20$, $d_{U_2,I} = 70$: (a) U_1 (64-QAM), (b) U_2 (16-QAM).

exhaustive search over a single discrete variable L_1. The third strategy (Joint opt.) is the joint optimization of both the transmit powers and L_1 using exhaustive search over L_1 and the PA scheme in Sec. VIII given each value of L_1. The figure shows that the second strategy, which only relies on optimizing L_1, leads to BER floors for both U_1 and U_2. The reason behind this is that increasing L_1 at the expense of L_2 to reduce the interference of U_2 on U_1 would harm the BER performance of U_2 and hence the average BER of the system. Figure 6(a) also shows that the third strategy offers a very slight performance gain for U_1 over the PA strategy with fixing $L_1 = L_2 = 35$. However, Fig. 6(b) shows that, for U_2, the situation is reversed and the PA strategy offers a slight performance gain over the joint optimization strategy. Therefore, we can conclude that the PA strategy is sufficient to optimize the system without further need to optimize the elements' allocation among the two users.

Figure 7 shows the BER performance of a two-user RIS-NOMA system under imperfect CSI knowledge at the BS. The figure clearly shows the impact of the quality of the estimated CSI, represented in ω, on the BER performance of the system. We can notice in Fig. 7 that BER floors exist due to the imperfect CSI which creates an irreducible noise, due to estimation error, whose power increases as the transmit powers increase, as shown in (47). As ω increases, the BER floor decreases to lower values, resulting in better performance for the system. We note that the source of the error floors in Fig. 7 is the channel estimation error, not the nature of uplink NOMA systems. However, even under imperfect CSI, the system can provide good performance with low BER levels due to applying the proposed PA scheme in Sec. VIII.

Figure 8 illustrates the impact of the number of BS antennas N on the BER performance of uplink NOMA transmission

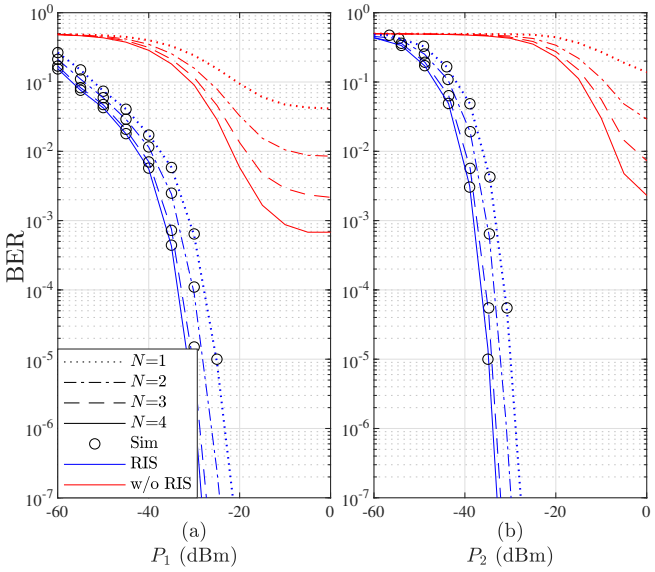

Figure 8: BER performance of a multi-antenna RIS-NOMA system with different numbers of BS antennas and $d_{U_1,I} = 20$, $d_{U_2,I} = 100$: (a) U_1 (64-QAM), (b) U_2 (16-QAM).

with and without the assistance of an RIS. It is observed that employing an RIS yields a remarkable performance enhancement compared to the case without RIS, where severe BER floors appear even at high SNR levels. In particular, without RIS, the BER floor decreases with increasing N, highlighting the role of spatial diversity in partially mitigating multi-user interference, yet the system still suffers from substantial error rates. In contrast, the RIS-assisted configuration consistently outperforms the baseline, achieving orders-of-magnitude lower BER and exhibiting steep performance gains as N increases. This confirms that integrating RIS not only suppresses the error floor but also leverages the array gain more effectively, thereby enabling reliable communication in uplink NOMA scenarios.

X. Conclusions

This paper investigated the achievable performance of uplink RIS-NOMA system, where users transmit their data to the BS using the same resource block and the BS employs SIC to detect the data symbols of each user. Closed-form expressions for the achievable BER were derived to provide useful insights about the performance limits of RIS-NOMA. The BER was compared to two TDMA-OMA counterparts to provide a comprehensive and fair comparison, where the first utilizes all partitions for each user at the expense of extra complexity, whereas the other assigns a partition to each user. Furthermore, a PA algorithm was introduced to mitigate the error floor imposed by the inter-user interference of uplink NOMA. Theoretical results corroborated by simulations revealed that RIS-NOMA is preferred over TDMA-OMA for almost all the considered SNR regimes. Furthermore, it was shown that by increasing the number of reflectors and/or increasing the modulation order, NOMA can have superior performance compared to both TDMA-OMA scenarios for a wide range, and in some cases the whole range, of the transmit power. The analysis and results also showed that imperfect CSI can cause error floors to the system performance; however, the level of these error floors decreases as the quality of the channel estimation increases. Finally, we showed through analysis and simulations how the BER performance can improve as the number of BS antennas increases.

Appendix A
Proof of Proposition 1

Let X be a RV and $g(x)$ be a real one-dimensional function. Then, the expected value, $\mathbb{E}[g(X)]$, can be calculated using the formula [46]

$$\mathbb{E}[g(x)] = \frac{1}{\pi}\int_0^{\infty} \mathfrak{Re}\left\{G(z)\Phi_X(z)\right\} dz, \tag{59}$$

where $G(z)$ is the Fourier transform (FT) of the function $g(x)$ and $\Phi_X(z)$ is the CF of the RV, X. Therefore, applying the above rule to average the conditional BER in (37), the average unconditional BER of U_k can be calculated as

$$BER_{U_k} = \sum_{q=1}^{N_k} \frac{c_{k,q}}{\pi}\int_0^{\infty} \mathfrak{Re}\left(\mathfrak{Q}(z)\Phi_{X_{k,q}}\left(\frac{z}{\sigma_n}\right)\right) dz, \tag{60}$$

where $\mathfrak{Q}(z)$ is the FT of the Q-function, which can be written as

$$\mathfrak{Q}(z) = \mathcal{F}(Q(t)) = \mathcal{F}\Big(\int_t^{\infty} e^{-y^2/2} dy\Big), \tag{61}$$

where $\mathcal{F}(\cdot)$ is the FT operator. Using the integral property of the FT in [47] and getting $\mathcal{F}(e^{-t^2/2})$ from the FT table, $\mathfrak{Q}(z)$ can be given as

$$\mathfrak{Q}(z) = \pi\delta(z) + j'\frac{e^{-z^2/2}}{z}, \tag{62}$$

where $\delta(\cdot)$ is the Dirac delta function. Substituting $\mathfrak{Q}(z)$ into (60), we can obtain the result of Proposition 1.

References

[1] M. Elbayoumi, M. Kamel, W. Hamouda, and A. Youssef, "NOMA-assisted machine-type communications in UDN: State-of-the-art and challenges," *IEEE Commun. Surv. Tutor.*, vol. 22, no. 2, pp. 1276–1304, Secondquarter 2020.

[2] O. Maraqa, A. S. Rajasekaran, S. Al-Ahmadi, H. Yanikomeroglu, and S. M. Sait, "A survey of rate-optimal power domain NOMA with enabling technologies of future wireless networks," *IEEE Commun. Surv. Tutor.*, vol. 22, no. 4, pp. 2192–2235, Fourthquarter 2020.

[3] S. M. R. Islam, N. Avazov, O. A. Dobre, and K.-S. Kwak, "Power-domain non-orthogonal multiple access (NOMA) in 5G systems: Potentials and challenges," *IEEE Commun. Surv. Tutor.*, vol. 19, no. 2, pp. 721–742, Secondquarter 2017.

[4] H. Yahya, A. Ahmed, E. Alsusa, A. Al-Dweik, and Z. Ding, "Error rate analysis of NOMA: Principles, survey and future directions," *IEEE Open J. Commun. Soc.*, vol. 4, pp. 1682–1727, Jul. 2023.

[5] M. A. ElMossallamy, H. Zhang, L. Song, K. G. Seddik, Z. Han, and G. Y. Li, "Reconfigurable intelligent surfaces for wireless communications: Principles, challenges, and opportunities," *IEEE Trans. Cogn. Commun. Netw.*, vol. 6, no. 3, pp. 990–1002, Sept. 2020.

[6] Y. Liu, X. Liu, X. Mu, T. Hou, J. Xu, M. Di Renzo, and N. Al-Dhahir, "Reconfigurable intelligent surfaces: Principles and opportunities," *IEEE Commun. Surv. Tutor.*, vol. 23, no. 3, pp. 1546–1577, Thirdquarter 2021.

[7] B. Zheng, C. You, W. Mei, and R. Zhang, "A survey on channel estimation and practical passive beamforming design for intelligent reflecting surface aided wireless communications," *IEEE Commun. Surv. Tutor.*, vol. 24, no. 2, pp. 1035–1071, Secondquarter 2022.

[8] R. Chen, M. Liu, Y. Hui, N. Cheng, and J. Li, "Reconfigurable intelligent surfaces for 6G IoT wireless positioning: A contemporary survey," *IEEE Internet Things J.*, vol. 9, no. 23, pp. 23 570–23 582, Dec. 2022.

[9] Q. Wu, S. Zhang, B. Zheng, C. You, and R. Zhang, "Intelligent reflecting surface-aided wireless communications: A tutorial," *IEEE Trans. Commun.*, vol. 69, no. 5, pp. 3313–3351, May 2021.
[10] Q. Wu and R. Zhang, "Intelligent reflecting surface enhanced wireless network via joint active and passive beamforming," *IEEE Trans. Wireless Commun.*, vol. 18, no. 11, pp. 5394–5409, Nov. 2019.
[11] C. Huang, A. Zappone, G. C. Alexandropoulos, M. Debbah, and C. Yuen, "Reconfigurable intelligent surfaces for energy efficiency in wireless communication," *IEEE Trans. Wireless Commun.*, vol. 18, no. 8, pp. 4157–4170, Aug. 2019.
[12] D. Zhao, H. Lu, Y. Wang, H. Sun, and Y. Gui, "Joint power allocation and user association optimization for IRS-assisted mmwave systems," *IEEE Trans. Wireless Commun.*, vol. 21, no. 1, pp. 577–590, Jan. 2022.
[13] M. AlaaEldin, E. Alsusa, and K. G. Seddik, "IRS-assisted physical layer network coding over two-way relay fading channels," *IEEE Trans. Veh. Technol.*, vol. 71, no. 8, pp. 8424–8440, Aug. 2022.
[14] M. Al-Jarrah, E. Alsusa, A. Al-Dweik, and D. K. C. So, "Capacity analysis of IRS-based UAV communications with imperfect phase compensation," *IEEE Wireless Commun. Lett.*, vol. 10, no. 7, pp. 1479–1483, Jul. 2021.
[15] J. Li, L. Yang, W. Hao, I. Ahmad, H. Liu, F. Shu, and D. Niyato, "Multi-layer transmitting RIS-aided receiver for collaborative jamming and anti-jamming networks," *IEEE Trans. Wireless Commun.*, vol. 24, no. 8, pp. 6518–6534, Aug. 2025.
[16] M. AlaaEldin, E. Alsusa, K. G. Seddik, M. Al-Jarrah, and C. B. Papadias, "Optimization of energy-constrained IRS-NOMA using a complex circle manifold approach," *IEEE Internet Things J.*, vol. 11, no. 20, pp. 33 133–33 150, Oct. 2024.
[17] Z. Ding, L. Lv, F. Fang, O. A. Dobre, G. K. Karagiannidis, N. Al-Dhahir, R. Schober, and H. V. Poor, "A state-of-the-art survey on reconfigurable intelligent surface-assisted non-orthogonal multiple access networks," *Proc. IEEE*, vol. 110, no. 9, pp. 1358–1379, Sept. 2022.
[18] Y. Liu, X. Mu, X. Liu, M. Di Renzo, Z. Ding, and R. Schober, "Reconfigurable intelligent surface-aided multi-user networks: Interplay between NOMA and RIS," *IEEE Wireless Commun.*, vol. 29, no. 2, pp. 169–176, Apr. 2022.
[19] B. Tahir, S. Schwarz, and M. Rupp, "Analysis of uplink IRS-assisted NOMA under Nakagami-m fading via moments matching," *IEEE Wireless Commun. Lett.*, vol. 10, no. 3, pp. 624–628, Mar. 2021.
[20] ——, "Outage analysis of uplink IRS-assisted NOMA under elements splitting," in *Proc. IEEE VTC*, Apr. 2021, pp. 1–5.
[21] Y. Cheng, K. H. Li, Y. Liu, K. C. Teh, and H. V. Poor, "Downlink and uplink intelligent reflecting surface aided networks: NOMA and OMA," *IEEE Trans. Wireless Commun.*, vol. 20, no. 6, pp. 3988–4000, Jun. 2021.
[22] B. Y. D. Rito and K. H. Li, "SER-effective constellation scaling and rotation in STAR-RIS-assisted uplink NOMA," *IEEE Commun. Lett.*, vol. 27, no. 9, pp. 2506–2510, Sept. 2023.
[23] Q. Li, M. El-Hajjar, Y. Sun, I. Hemadeh, A. Shojaeifard, Y. Liu, and L. Hanzo, "Achievable rate analysis of the STAR-RIS-aided NOMA uplink in the face of imperfect CSI and hardware impairments," *IEEE Trans. Commun.*, vol. 71, no. 10, pp. 6100–6114, Oct. 2023.
[24] T. Wang, M.-A. Badiu, G. Chen, and J. P. Coon, "Outage probability analysis of STAR-RIS assisted NOMA network with correlated channels," *IEEE Commun. Lett.*, vol. 26, no. 8, pp. 1774–1778, Aug. 2022.
[25] X. Yue and Y. Liu, "Performance analysis of intelligent reflecting surface assisted NOMA networks," *IEEE Trans. Wireless Commun.*, vol. 21, no. 4, pp. 2623–2636, Apr. 2022.
[26] A. Chauhan, S. Ghosh, and A. Jaiswal, "RIS partition-assisted non-orthogonal multiple access (NOMA) and quadrature-NOMA with imperfect SIC," *IEEE Trans. Wireless Commun.*, vol. 22, no. 7, pp. 4371–4386, Jul. 2023.
[27] U. Singh, H. Al-Tous, O. Tirkonnen, and M. R. Bhatnagar, "Performance analysis of the STAR-RIS-assisted downlink NOMA communication system with MRC," *IEEE Commun. Lett.*, vol. 27, no. 7, pp. 1739–1743, Jul. 2023.
[28] Z. Han, X. Yue, B. Dai, R. Liu, and A. Nallanathan, "Reconfigurable intelligent surface assisted unified NOMA framework," *IEEE Trans. Veh. Technol.*, vol. 72, no. 8, pp. 10 617–10 632, Aug. 2023.
[29] V. C. Thirumavalavan and T. S. Jayaraman, "BER analysis of reconfigurable intelligent surface assisted downlink power domain NOMA system," in *Proc. IEEE COMSNETS*, Jan. 2020, pp. 519–522.
[30] L. Bariah, S. Muhaidat, P. C. Sofotasios, F. E. Bouanani, O. A. Dobre, and W. Hamouda, "Large intelligent surface-assisted nonorthogonal multiple access for 6G networks: Performance analysis," *IEEE Internet Things J.*, vol. 8, no. 7, pp. 5129–5140, Apr. 2021.
[31] A. T. Dogukan, E. Arslan, and E. Basar, "Reconfigurable intelligent surface-enabled downlink NOMA," *IEEE Trans. Wireless Commun.*, vol. 23, no. 11, pp. 16 950–16 961, Nov. 2024.
[32] L. Wei, C. Huang, G. C. Alexandropoulos, C. Yuen, Z. Zhang, and M. Debbah, "Channel estimation for RIS-empowered multi-user MISO wireless communications," *IEEE Trans. Commun.*, vol. 69, no. 6, pp. 4144–4157, Jun. 2021.
[33] Q.-U.-A. Nadeem, H. Alwazani, A. Kammoun, A. Chaaban, M. Debbah, and M.-S. Alouini, "Intelligent reflecting surface-assisted multi-user MISO communication: Channel estimation and beamforming design," *IEEE Open J. Commun. Soc.*, vol. 1, pp. 661–680, May 2020.
[34] Y. Liu, S. Zhang, F. Gao, J. Tang, and O. A. Dobre, "Cascaded channel estimation for RIS assisted mmWave MIMO transmissions," *IEEE Wireless Commun. Lett.*, vol. 10, no. 9, pp. 2065–2069, Sept. 2021.
[35] S. Atapattu, R. Fan, P. Dharmawansa, G. Wang, J. Evans, and T. A. Tsiftsis, "Reconfigurable intelligent surface assisted two–way communications: Performance analysis and optimization," *IEEE Trans. Commun.*, vol. 68, no. 10, pp. 6552–6567, Oct. 2020.
[36] A. Papoulis and U. Pillai, *Probability, Random Variables and Stochastic Processes*, 4th ed. McGraw-Hill, Nov. 2001.
[37] K. V. Mardia and P. E. Jupp, *Directional Statistics*, 1st ed. Wiley, Jan. 1999.
[38] T. F. Coleman and Y. Li, "An interior trust region approach for nonlinear minimization subject to bounds," *SIAM J. Optim.*, vol. 6, no. 2, pp. 418–445, May 1996.
[39] J. E. Dennis, M. El-Alem, and K. Williamson, "A trust-region approach to nonlinear systems of equalities and inequalities," *SIAM J. Optim.*, vol. 9, no. 2, pp. 291–315, Jan. 1999.
[40] J. J. Moré, "The Levenberg-Marquardt algorithm: Implementation and theory," in *Numerical Analysis*, G. A. Watson, Ed., vol. 630. Springer Berlin Heidelberg, Aug. 2006, pp. 105–116.
[41] H. Yahya, E. Alsusa, and A. Al-Dweik, "Exact BER analysis of NOMA with arbitrary number of users and modulation orders," *IEEE Trans. Commun.*, vol. 69, no. 9, pp. 6330–6344, Sept. 2021.
[42] Q. Li, M. El-Hajjar, I. Hemadeh, D. Jagyasi, A. Shojaeifard, and L. Hanzo, "Performance analysis of active RIS-aided systems in the face of imperfect CSI and phase shift noise," *IEEE Trans. Veh. Technol.*, vol. 72, no. 6, pp. 8140–8145, Jun. 2023.
[43] P. Yang, L. Yang, and S. Wang, "Performance analysis for RIS-aided wireless systems with imperfect CSI," *IEEE Wireless Commun. Lett.*, vol. 11, no. 3, pp. 588–592, Mar. 2022.
[44] S. Hong, C. Pan, H. Ren, K. Wang, K. K. Chai, and A. Nallanathan, "Robust transmission design for intelligent reflecting surface-aided secure communication systems with imperfect cascaded CSI," *IEEE Trans. Wireless Commun.*, vol. 20, no. 4, pp. 2487–2501, Apr. 2021.
[45] X. Mu, Y. Liu, L. Guo, J. Lin, and N. Al-Dhahir, "Exploiting intelligent reflecting surfaces in NOMA networks: Joint beamforming optimization," *IEEE Trans. Wireless Commun.*, vol. 19, no. 10, pp. 6884–6898, Oct. 2020.
[46] A. Annamalai, C. Tellambura, and V. Bhargava, "A general method for calculating error probabilities over fading channels," *IEEE Trans. Commun.*, vol. 53, no. 5, pp. 841–852, May 2005.
[47] B. Davies, *Integral Transforms and Their Applications*, 3rd ed. Springer New York, NY, Jan. 2002.

Mahmoud AlaaEldin (Member, IEEE) is an Associate Fellow of the UK Higher Education Academy (AFHEA). He received the B.Sc. degree in electrical engineering from Alexandria University, Alexandria, Egypt, in 2013, and the M.Sc. degree in electronics and communications engineering from the American University in Cairo (AUC), Cairo, Egypt, in 2019. He received his Ph.D. degree in electrical and electronics engineering from The University of Manchester, Manchester, UK, in 2024. He is currently a research fellow with the Centre for Wireless Innovation (CWI) at Queen's University Belfast (QUB).

Dr. AlaaEldin received a University Fellowship from AUC during his M.Sc. studies, and the Marie Skłodowska-Curie Actions (MSCA) fellowship from the European Union (EU), under the EU's Horizon 2020 research and innovation program, during his Ph.D. His research interests span diverse topics in wireless communications and signal processing including multi-user MIMO/OFDM systems, massive MIMO systems, channel estimation and feedback, reconfigurable intelligent surfaces (RISs), integrated sensing and communications, near field communications, pinching and flexible antenna systems, optimization of wireless systems, and applications of machine learning in wireless communications and signal processing.

Mohammad Al-Jarrah (Member, IEEE) received the B.Sc. and M.Sc. degrees in electrical engineering/wireless communications from Jordan University of Science and Technology, Irbid, Jordan, in 2008 and 2011, respectively, and the Ph.D. degree in electrical and electronics engineering from The University of Manchester, Manchester, U.K., in 2023. He is currently a Postdoctoral Research Assistant with the University of Manchester. His research interests include diverse topics in wireless communications and signal processing: distributed decision fusion systems, statistical signal processing, localization and tracking, RFID communications, spectrum sensing, integrated radar-communications, intelligent reflecting surfaces (IRSs), and machine learning for signal processing applications. He is a recipient of the Royal Jordanian Scholarship and Marie Sklodowska-Curie Actions (MSCA) fellowship from the European Union.

Xidong Mu (Member, IEEE, https://xidongmu.github.io/) has been a lecturer (an assistant professor) with the Centre for Wireless Innovation (CWI), School of Electronics, Electrical Engineering and Computer Science, Queen's University Belfast, U.K. since August 2024. His research interests include flexible-antenna technologies, reconfigurable surface aided communications, next generation multiple access (NGMA), integrated sensing and communications, and optimization theory. He is a Web of Science Highly Cited Researcher. He received the IEEE ComSoc Outstanding Young Researcher Award for EMEA region in 2023 and the IEEE ComSoc Wireless Communications Technical Committee (WTC) Outstanding Young Researcher Award in 2025. He is the recipient of the 2024 IEEE Communications Society Heinrich Hertz Award, the Best Paper Award in ISWCS 2022, the 2022 IEEE Signal Processing and Computing for Communications Technical Committee (SPCC-TC) Best Paper Award, and the Best Student Paper Award in IEEE VTC2022-Fall. He serves as the secretary of the IEEE ComSoc Technical Committee on Cognitive Networks (TCCN), the secretary of the IEEE ComSoc SPCC-TC, and the URSI UK Early Career Representative (ECR) for Commission C. He also serves as an Editor of IEEE TCOM, a Guest Editor for IEEE JSAC, IEEE TCCN, IEEE IoT-J, and the "Mobile and Wireless Networks" symposium co-chair of IEEE GLOBECOM 2025.

Emad Alsusa (Senior Member, IEEE) is a Professor of Communications and Signal Processing at the University of Manchester, where he also leads the Communications Research Group. He obtained his PhD in Telecommunications from the University of Bath, UK, in 2000 and subsequently worked on high-data-rate systems as part of an industrial project at the University of Edinburgh. He joined Manchester University in 2003, where he has since made significant contributions to the field. Emad's research focuses on communication systems, spanning the physical, MAC, and network layers. His work involves developing advanced techniques and algorithms, including array signal detection, channel estimation, equalization, adaptive signal precoding, interference mitigation, radio resource management, and energy and spectrum optimization. His research has been applied in various domains, including cellular networks, IoT, Industry 4.0, vehicular networks, and powerline communications. He has authored over 300 peer-reviewed journal and conference publications, many of which appear in leading IEEE transactions and conferences. Over his career, he has successfully supervised more than 40 PhD students. Emad serves as an Editor for IEEE Wireless Communications Letters and IEEE Transactions on Vehicular Technology. He has also contributed to the research community in various leadership roles, including as TPC Track Chair for VTC'16, GISN'16, PIMRC'17, and Globecom'18, and as General Co-Chair for the OnlineGreenCom'16 Conference. Additionally, he represents the UK in the International Union of Radio Science (URSI) and co-chairs the IEEE Special Working Group on RF Energy Harvesting. His work has been recognized with several prestigious awards, including Best Paper Awards at the International Symposium on Power Line Communications (ISPLC) 2016 and the IEEE Wireless Communications and Networks Conference (WCNC) 2019.

Karim G. Seddik (Senior Member, IEEE) received the B.Sc. (Hons.) and M.Sc. degrees in electrical engineering from Alexandria University, Alexandria, Egypt, in 2001 and 2004, respectively, and the Ph.D. degree from the University of Maryland, College Park, MD, USA, in 2008.

He is currently a Professor at the Electronics and Communications Engineering Department at the American University in Cairo (AUC), where he is also an Associate Dean of Graduate Studies and Research in the School of Sciences and Engineering. Before joining AUC, he was an Assistant Professor at Alexandria University. His research interests include applications of machine learning in communication networks, intelligent reflecting surfaces, age of information, and backscattered communications.

He was a recipient of the American University in Cairo Faculty Merit Award for Excellence in Research and Creative Endeavors in 2021, the State Encouragement Award in 2016, the State Medal of Excellence in 2017, and the Certificate of Honor from the Egyptian President for being ranked first among all departments in the College of Engineering at Alexandria University in 2002. He received the Graduate School Fellowship in 2004 and 2005 and the Future Faculty Program Fellowship in 2017 from the University of Maryland. He co-authored a journal paper that received the IEEE Communications Society Best Tutorial Paper Award in 2025. He also co-authored a conference paper that received the Best Conference Paper Award from the IEEE Communication Society Technical Committee on Green Communications and Computing in 2019. He currently serves as an Editor for the IEEE TRANSACTIONS ON MACHINE LEARNING IN COMMUNICATIONS AND NETWORKING. He has served on the technical program committees for numerous IEEE conferences in the areas of wireless networks and mobile computing.

Michail Matthaiou (Fellow, IEEE) obtained his Ph.D. degree from the University of Edinburgh, U.K. in 2008. He is currently a Professor of Communications Engineering and Signal Processing and Deputy Director of the Centre for Wireless Innovation (CWI) at Queen's University Belfast, U.K. He is also an Eminent Scholar at the Kyung Hee University, Republic of Korea. He has held research/faculty positions at Munich University of Technology (TUM), Germany and Chalmers University of Technology, Sweden. His research interests span signal processing for wireless communications, beyond massive MIMO, reflecting intelligent surfaces, mm-wave/THz systems and AI-empowered communications.

Dr. Matthaiou and his coauthors received the IEEE Communications Society (ComSoc) Leonard G. Abraham Prize in 2017. He currently holds the ERC Consolidator Grant BEATRICE (2021-2026) focused on the interface between information and electromagnetic theories. To date, he has received the prestigious 2023 Argo Network Innovation Award, the 2019 EURASIP Early Career Award and the 2018/2019 Royal Academy of Engineering/The Leverhulme Trust Senior Research Fellowship. His team was also the Grand Winner of the 2019 Mobile World Congress Challenge. He was the recipient of the 2011 IEEE ComSoc Best Young Researcher Award for the Europe, Middle East and Africa Region and a co-recipient of the 2006 IEEE Communications Chapter Project Prize for the best M.Sc. dissertation in the area of communications. He has co-authored papers that received best paper awards at the 2018 IEEE WCSP and 2014 IEEE ICC. In 2014, he received the Research Fund for International Young Scientists from the National Natural Science Foundation of China. He is currently the Editor-in-Chief of Elsevier Physical Communication, a Senior Editor for IEEE WIRELESS COMMUNICATIONS LETTERS and IEEE SIGNAL PROCESSING MAGAZINE, an Area Editor for IEEE TRANSACTIONS ON COMMUNICATIONS and Editor-in-Large for IEEE OPEN JOURNAL OF THE COMMUNICATIONS SOCIETY. He is an IEEE and AAIA Fellow.